BRNO UNIVERSITY OF TECHNOLOGY
VYSOKÉ UČENÍ TECHNICKÉ V BRNĚ

FACULTY OF ELECTRICAL ENGINEERING AND COMMUNICATION
FAKULTA ELEKTROTECHNIKY
A KOMUNIKAČNÍCH TECHNOLOGIÍ

DEPARTMENT OF MICROELECTRONICS
ÚSTAV MIKROELEKTRONIKY

IMPLEMENTATION OF A MULTIPURPOSE MEASUREMENT SYSTEM FOR (SUB)TERAHERTZ ELECTRON SPIN RESONANCE SPECTROSCOPY

REALIZACE VÍCEÚČELOVÉHO MĚŘÍCÍHO SYSTÉMU PRO (SUB)TERAHERTZOVOU ELEKTRONOVOU SPINOVOU REZONANČNÍ SPEKTROSKOPII

DOCTORAL THESIS
DIZERTAČNÍ PRÁCE

AUTHOR
AUTOR PRÁCE
Ing. Matúš Šedivý

SUPERVISOR
ŠKOLITEL
prof. Ing. Radimír Vrba, CSc.

CO-SUPERVISORS
ŠKOLITELÉ SPECIALISTI
doc. Ing. Petr Neugebauer Ph.D.
and Dr. Oleksii Laguta

BRNO 2024

Abstract

Electron spin resonance (also called electron paramagnetic resonance or just EPR) spectroscopy includes methods that investigate matter via unpaired electrons. One of the progressive EPR methods is the rapid scan, which allows one to observe the kinetics of chemical reactions. Moreover, recent developments of high-frequency components expand application of high-frequency EPR (HFEPR), that use sub-terahertz and terahertz waves. This thesis deals with the connection of both paths into the frequency rapid scan (FRaScan) HFEPR spectrometer that was recently developed at CEITEC BUT. A brief introduction to the theoretical background of EPR is provided, followed by an overview of the HFEPR instrumentation. The practical part describes a technical solution for the spectrometer. The emphasis is on the implementation of software through which the spectrometer is controlled, and measurements are automated. Afterward are shown example measurements of solid state materials, namely vanadium doped silicon carbide (SiC:V), lithium phthalocyanine (LiPc), and crystal of 1,3-bisdiphenylene-2-phenylallyl (BDPA). The examples demonstrate the capabilities of the spectrometer to acquire multi-frequency continuous wave spectra and frequency-swept spectra with dependency on the temperature and orientation of the sample, as well as the frequency rapid scan spectra.

Keywords

Electron-spin resonance, spectroscopy, spectrometer, magnetic resonance, development, instrument, experimental setup, prototype, terahertz beams, rapid scan, defects in crystals, qubit, silicon carbide, software, LabVIEW, simulation

Contents

Introduction 3
1 Brief theory of the EPR 5
1.1 Mathematical description of electron spin resonance phenomenon 7
1.2 General EPR instrumentation 9
1.3 Pulse EPR spectroscopy 12
1.4 Rapid scan 14
1.5 Current software solutions for EPR spectroscopy 16
2 Equipment for HFEPR spectroscopy 19
2.1 Electromagnets and superconducting magnets 19
2.2 Millimeter and submillimeter wave sources 20
2.3 Detectors in Terahertz region 21
2.4 Quasi optics 21
3 FRaScan HFEPR spectrometer 22
3.1 Description of spectrometer 22
3.2 EPR probes and sample holders 25
3.3 Modes of operation 27
3.4 Software solution 28
3.5 Implementation of frequency rapid scan 33
4 Solid state materials studied by HF-EPR 35
4.1 HF-EPR study of SiC doped by Vanadium 35
4.2 FS-EPR measurements and EPR maps 37
4.3 Rotation measurements 40
4.4 FRaScan measurements 41
Conclusion 42
Literature references 43

Introduction

Electron spin resonance (ESR) spectroscopy, also called electron paramagnetic resonance (EPR) or electron magnetic resonance (EMR) spectroscopy, allows studying materials with unpaired electrons. It is a technique similar to nuclear magnetic resonance (NMR), both are based on interaction of electromagnetic wave with magnetic dipole moment, but in EPR the origin of the magnetic dipole is the electron, not the nuclei. The EPR is a widely used technique in chemistry, biology, and physics where it provides information on the structure and dynamics of free radicals to understand the kinetics of chemical reactions, oxidation and reduction processes, catalysis, photosynthesis, enzyme reactions, the behavior of antioxidants, photochemical reactions, radiation effect on biological compounds, organic conductors, migration of electrical charge carriers and defects in materials [1]. Apart from basic research, there are several industrial applications of EPR. For example, packaging materials in the food industry are irradiated for sterilization. By measuring the specific radical concentration using EPR, it is possible to judge, the appropriate dose of radiation. Another example of industrial application is the monitoring of antioxidants in beer samples, which protects it from premature staling [2]. Besides these, there is significant progress in the research of medical applications similar to magnetic resonance imaging (MRI) called EPR imaging [3], which can be used also for non-living objects as batteries, to monitor redox reactions on its electrodes [4]. It is also a key method for research and development in spintronics [5, 6]. Examples of material research can be found in semiconductor materials based on silicon carbide, which can be used in photovoltaic cells, where EPR allows to study of their defects and impurities [7]. EPR can be also used in the investigation of thin film materials [8]. Pulsed EPR methods are mostly used to study the structure of biomolecules [9]. Finally, a high-frequency EPR technique is needed in the research of single molecular magnets [10].

EPR was first observed in 1944 by Evgeny Zavoisky on a sample of $MnSO_4$. He was focused to study of the physical and chemical impact of ultrashort waves on matter in laboratories of Kazan State University. His aim was to improve nuclear magnetic resonance experiments. However, his work was interrupted because of the Second World War. At the end of 1943, he changed his focus to electron spins. He measured the absorption coefficient of the radiofrequency field as a function of static magnetic field in solutions of manganese salts. Zavoisky demonstrated that the ratio of radio wave frequency and static magnetic field corresponding to the absorption maximum was constant. Moreover, it was in agreement with the expected value, of the energy difference of a magnetic dipole transition between quantum states of electron spins [11]. The reconstruction of Zavoisky's experimental setup is in Figure 1. Another pioneer in EPR was Brebis Bleaney who was looking for possibilities of using the recently developed microwave technology. His first EPR experiments were done in 1946 at the University of Oxford, unaware of Zavoisky's work. Results of these experiments showed that the

broadening of spectral lines could be reduced by using cryogenic temperatures and dilution of samples [12].

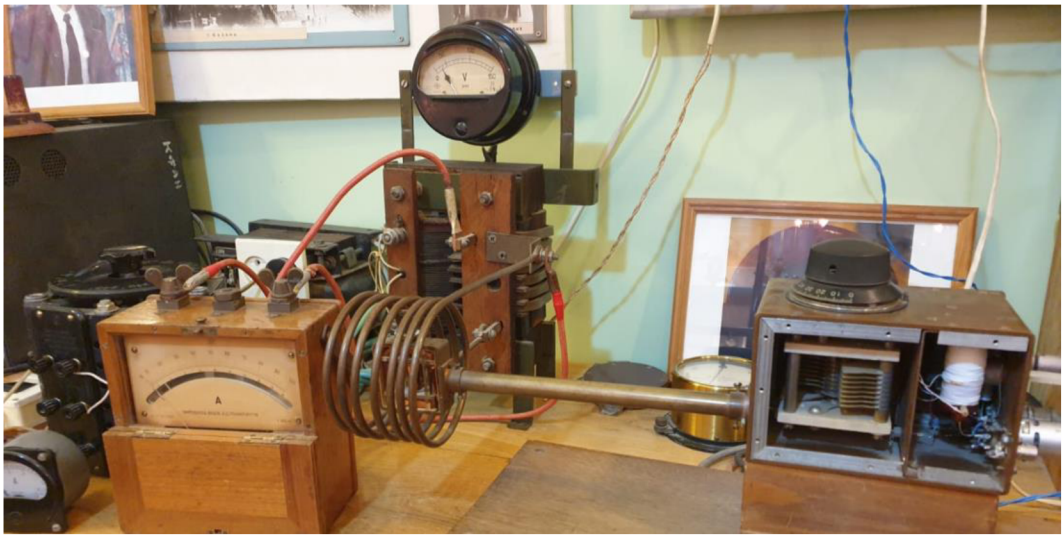

Figure 1: Reconstruction of EPR experimental setup in Evgeny Zavoisky Lab-Museum in Kazan. Photo made by Petr Neugebauer (11.03.2021).

During the second half of the 20th century, EPR spectroscopy significantly evolved, and the range of its applications has broadened from analytical and physical chemistry to biology and medicine. The technological advances allowed to the improve precision and sensitivity of EPR spectrometers and make a large variety of experimental setups. The first multi-frequency, high-frequency, and pulsed EPR spectrometers were developed [13, 14]. A few companies started to produce and sell EPR spectrometers (Bruker, Magnettech, JEOL). Although, even nowadays new ways for EPR spectroscopy are explored. One of the revolutionary approaches is EPR-on-a-chip (EPRoC) developed at the Institute of Smart Sensors at the University of Stuttgart. It focuses on the miniaturization and integration of EPR instrumentation in a single chip (excluding electromagnet), that to be mass-produced and consequently suitable for low-cost and portable EPR applications [15]. Electrically-detected magnetic resonance (EDMR) is another approach to conduct EPR by detection of changes in conductivity. This technique is more suitable for solid state materials for determination of intrinsic properties such as density and charge carrier mobility. Moreover, newer microwave technologies allowed the development of high-frequency spectrometers that can operate at higher frequencies of the sub-terahertz region and with a broader range. Another cutting-edge pathway in EPR spectroscopy is a rapid scan EPR – a revolutionary method developed by an Eaton group at the University of Denver. It significantly improves signal-to-noise ratio and decrease acquisition time [16]. Finaly, the EPR also drives further development in NMR via so called a dynamic nuclear polarization (DNP), that offers promising opportunities to significantly enhance NMR sensitivity and expand the capabilities of NMR spectroscopy.

1 Brief theory of the EPR

One of the quantum mechanics properties of elementary particles is a spin. It is an intrinsic form of angular momentum. For a single electron, the spin angular momentum S is equal to ½, and the spin quantum number m_s has a value ±½ (according to its orientation). The spin angular momentum is then ½ multiple of the reduced Planck constant $\hbar$. Because the electron is a particle that carries an electrical charge q, due to the spin, it behaves as a current loop which exhibits magnetic momentum called spin magnetic momentum μ_s that is proportional to spin angular momentum. Via gyromagnetic ratio γ we can calculate the spin magnetic momentum of a free electron

$$\mu_{\boldsymbol{s}} = \gamma\hbar\boldsymbol{S} = g\frac{q}{2m_e}\hbar\boldsymbol{S} = -g_e\beta_e\boldsymbol{S} \ \ [\mathrm{J}\cdot\mathrm{T}^{-1}], \tag{1}$$

where m_e is the mass of electron $9.1094\cdot10^{-31}$ kg, q is elementary charge $1.6022\cdot10^{-19}$ C, β_e is Bohr magneton whose value is $9.274\cdot10^{-24}$ J·T^{-1}, and g_e is a dimensionless parameter called g-factor of a free electron and its value is about 2.0023 [17].

In materials that contain unpaired electrons (paramagnetic centers), spin magnetic moments have randomly distributed orientations and cancel each other because of heat (k_bT, where k_b is Boltzmann constant $1.381\cdot10^{-23}$ J·K^{-1}, and T is absolute temperature). Such material is called paramagnetic and without an external magnetic field, both spin orientations (½ and -½) share the same energy level (energy levels are degenerated). However, in the presence of a static external magnetic field, spin magnetic moments tend to orient parallel to the direction of the external field B_0 because it is energetically favorable (and less favorable in antiparallel direction) in terms of their potential energy. Under the influence of the magnetic field, the energy levels for both spin orientations (½ and -½) split, which is called the **Zeeman effect**, as shown in Figure 2. A shift from degenerated energy level for each orientation is defined as:

$$E = m_s g\beta_e B_0 \ \ [\mathrm{J}], \tag{2}$$

then the difference between energy levels is:

$$\Delta E = \frac{1}{2}g\beta_e B_0 - \left(-\frac{1}{2}g\beta_e B_0\right) = g\beta_e B_0 \ \ [\mathrm{J}], \tag{3}$$

where B_0 is the external magnetic field (also called a flux density or induction) and g is a factor which in most materials slightly differs from g_e because of contributions such as spin-orbital coupling and thus is characteristic for each paramagnetic species [17, 18].

By applying radiation with the magnetic component B_1 perpendicular to the static magnetic field, which energy of photons meets the energy difference between different spin states, causing the electron spin resonance. A fundamental equation that expresses a resonance condition in electron paramagnetic resonance spectroscopy is:

$$hf = g\beta_e B_0 \ \ [\mathrm{J}] \tag{4}$$

where hf is the energy of the photon (h – Planck constant, f – frequency).

Meeting this condition will cause an absorption of radiation that can be interpreted as the intensity of a spectral line. Another way to achieve electron spin resonance is by applying microwave radiation of constant frequency and adjusting the magnetic field. This approach is technically easier to achieve, by simply changing electrical current through a coil [19]. Technical aspects of EPR spectrometers will be discussed later in section 1.2.

If an atom with non-zero nuclear spin is present near the paramagnetic center, so-called hyperfine splitting of energy levels effectively occurs. It arises from the interaction between electronic spin S and nuclear spin I. A simple example can be presented on a single hydrogen atom (hydrogen molecule has paired electrons). It has one valence electron with spin S= ½ and a single proton also gives nuclear spin I= ½ (deuterium has I= 1). Without an external magnetic field, both electron spin states (m_s= ±½) share the same energy level. However, in the magnetic field, sublevel m_s= +½ is going up, and sublevel m_s= -½ is going down. At each sublevel, electron spin interacts with both nuclear spin states (m_I= ±½) giving four energy sublevels. Their energy can be calculated by equation:

$$E = m_s g\beta B + A m_s m_I \tag{5}$$

where m_I is the nuclear quantum spin number, and A is a hyperfine coupling constant.

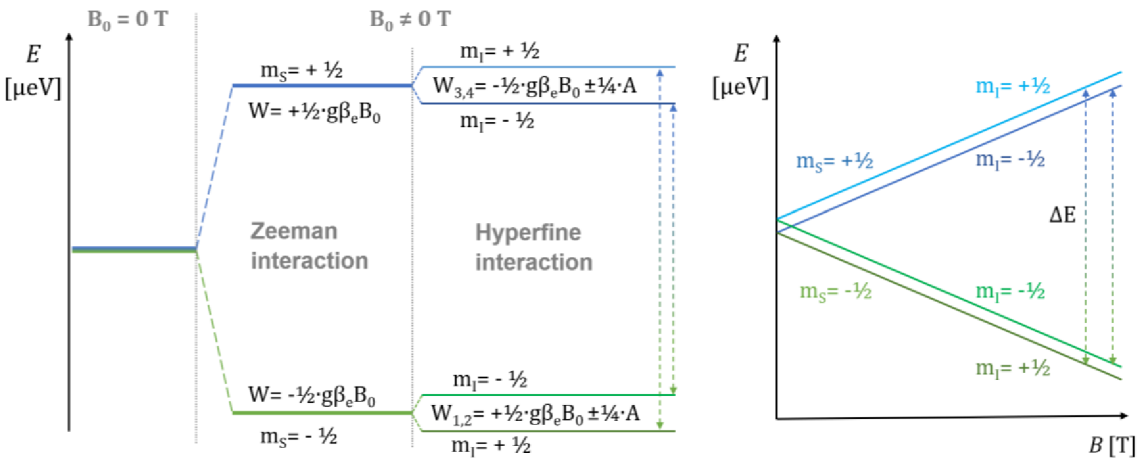

Figure 2: Splitting of energy levels and allowed EPR transitions between them in static magnetic field (left) and linearly varying magnetic field (right) for a hydrogen example.

In cases of multiple equivalent nuclei n_i, or when nuclear spin is more than ½ (I= 1, 3/2, 2…), the number of possible spin transitions will be:

$$N_t = 2 \cdot n_i \cdot I + 1 \tag{6}$$

If n_i > 1, intensity ratio follows Pascal triangle (1, 1:1, 1:2:1, 1:3:3:1, ...).

1.1 Mathematical description of electron spin resonance phenomenon

To simulate EPR spectra, the concept of an **effective spin Hamiltonian** is used for the description of spin interactions as well as for the system reaction to the external magnetic field. However, the spin Hamiltonian model may not be valid for cases with large spin-orbital coupling or samples in the gas phase. The spin Hamiltonian operator relates to the total energy of a spin system and consists of sums of interaction terms:

$$\hat{H} = \sum_i(\hat{H}_{ez,i} + \hat{H}_{zf,i}) + \sum_{i,j}\hat{H}_{ss,ij} + \sum_{i,k}\hat{H}_{hf,ik} + \sum_k(\hat{H}_{nz,i} + \hat{H}_{nq,i}). \qquad (7)$$

for example, $\hat{H}_{ez}$ is a term for electron Zeeman interaction:

$$\hat{H}_{ez} = \beta \boldsymbol{B}^T \tilde{\boldsymbol{g}}\hat{\boldsymbol{S}} = \beta\left(g_{xx}B_x\hat{S}_x + g_{yy}B_y\hat{S}_y + g_{zz}B_z\hat{S}_z\right). \qquad (8)$$

Other terms express Hamiltonian components for: zero-field splitting H_{zf}, spin-spin interaction H_{ss}, hyperfine splitting H_{hf}, nuclear Zeeman interaction H_{nz} and H_{nq} is the nuclear electric quadrupole.

$$\hat{H}_{zf} = \hat{\boldsymbol{S}}^T\boldsymbol{D}\hat{\boldsymbol{S}}, \qquad \hat{H}_{ss} = \hat{\boldsymbol{S}}_1^T\boldsymbol{J}\hat{\boldsymbol{S}}_2, \qquad \hat{H}_{hf} = \hat{\boldsymbol{S}}^T\boldsymbol{A}\hat{\boldsymbol{I}}, \qquad \hat{H}_{nq} = \hat{\boldsymbol{I}}^T\boldsymbol{Q}\hat{\boldsymbol{I}}. \qquad (9)$$

Here $\hat{\boldsymbol{S}}$ is an operator of the electron spin, $\tilde{\boldsymbol{I}}$ is an operator of the nuclear spin, $\boldsymbol{J}$ is a coupling matrix, $\boldsymbol{D}$ is the zero-field tensor, $\boldsymbol{Q}$ is the traceless nuclear quadrupole tensor and $\boldsymbol{A}$ is the hyperfine coupling matrix. Calculation of total spin Hamiltonian might be very demanding. Further explanation of spin Hamiltonian can be found in the literature [17, 20, 21].

The reaction of a material to an applied magnetic field is described by its **magnetization**, which is a vector that represents the volume density of oriented magnetic dipole moments. From the classical point of view, magnetization can be expressed by the equation:

$$\boldsymbol{M} = \frac{\boldsymbol{B}}{\mu_0} - \boldsymbol{H} = \mu_r\boldsymbol{H} - \boldsymbol{H} = (\mu_r - 1)\boldsymbol{H} = \chi\mathbf{H}\ [\mathrm{A}\cdot\mathrm{m}^{-1}]. \qquad (10)$$

where $\boldsymbol{H}$ is a vector of the magnetic field intensity, μ_r is the permeability of vacuum, μ_r is relative permeability and χ is the magnetic susceptibility of a material. Alternatively, magnetization can be expressed as a collection of N dipoles in a given volume V which results in a macroscopic moment:

$$\boldsymbol{M} = \frac{1}{V}\sum_{i=1}^{N}\boldsymbol{\mu}_i = \frac{d\boldsymbol{\mu}}{dV}\ [\mathrm{J}\cdot\mathrm{T}^{-1}\mathrm{m}^{-3}], \qquad (11)$$

where $d\boldsymbol{\mu}$ is the elementary magnetic dipole moment and dV is a volume element. As the magnetization reflects a bulk response of a large number of spins, it can hide the detailed behavior of single spins but also allows to avoid a quantum mechanical treatment of the resonance phenomenon [17].

As mentioned above, if paramagnetic material is in the external magnetic field, energy levels for spin states -½ and +½ will split, and their energy difference is linearly proportional to the magnetic field. Because the potential energy for the spin states pointing antiparallel to the magnetic field is lower (in the case of the electron), we can expect a higher density of states at this energy level for thermodynamic equilibrium. According to Boltzmann distribution, the ratio between these states will be:

$$\frac{N_u}{N_l} = \exp\left(-\frac{\Delta E}{\mathrm{k_b} T_s}\right) = \exp\left(-\frac{g\beta_e B_0}{\mathrm{k_b} T_s}\right), \tag{12}$$

Where N_u and N_l are respectively the density of states in the upper and lower levels, ΔE is the energy difference of levels (3), $\mathrm{k_b}$ is a Boltzmann constant ($1.3806 \cdot 10^{-23}$ $\mathrm{J \cdot K^{-1}}$), and T_s is a parameter called spin temperature, that may be considered equal to surrounding temperature in case of thermodynamic equilibrium. In practice, this means that at room temperature the difference between states at the upper and lower level is usually very small. However, it will increase with lower temperature, which will reduce spontaneous transitions. Also, at the higher magnetic field, the ΔE will linearly increase. And that will consequently result in better sensitivity.

Radiation that meets the EPR condition by equation (4) will cause an excitation/transition of states from the lower level to the upper level. This leads to a change in the population of both energy levels and to distortion of thermodynamic equilibrium. The population change (caused by the absorption of photons) is proportional to the power of the radiation. Electron spins that are excited to higher energy levels tend to return to the state with lower potential energy by losing energy to the surroundings (by phonons and photons), to achieve thermodynamic equilibrium. This process is called spin relaxation. A loss of an excess energy follows an exponential decay:

$$\delta E = \delta E_0 \exp\left(-\frac{t - t_0}{\tau}\right), \tag{13}$$

where δE_0 is an excess energy at time t_0, and τ is the characteristic time for energy flow from the spin system into surroundings and is related to the mean lifetime of a given spin-orientation state (see Figure 3) [17]. If the power of the radiation is too large or the relaxation time is too long, the relaxation does not keep up, and the spin package is saturated. Then, the change in population is no longer proportional to radiation power.

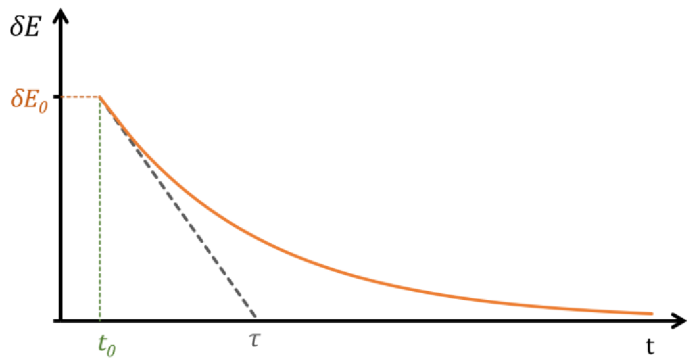

Figure 3: Exponential decay of excess energy.

Because the magnetization $\boldsymbol{M}$ along the externally applied magnetic field is proportional to the population difference in spin states, it is possible to use a macroscopic model of the spin relaxation to describe the time dependence of total spin magnetization vector $\boldsymbol{M}$. This mathematical tool is called **Bloch equations**. It is useful for the interpretation of the magnetic-resonance phenomenon in terms of vectors and torques, which helps to understand the effect of microwave pulses. It also simplifies the complexity of spin interaction with surroundings by using relaxation times τ_1 and τ_2 as empirical parameters. Explanation of absorption and dispersion concepts can also be obtained by the Bloch equations. They omit the quantum-mechanical behavior of individual spins without loss of generality. A form of the Bloch equations that consider the response of magnetization to sudden change of homogenous magnetic field is

$$\frac{dM_x}{dt} = \gamma_e B M_y - \frac{M_x}{\tau_2} \tag{14}$$

$$\frac{dM_y}{dt} = -\gamma_e B M_x - \frac{M_y}{\tau_2} \tag{15}$$

$$\frac{dM_z}{dt} = \frac{M_z^0 - M_z}{\tau_1} \quad . \tag{16}$$

Here indexes are used for individual components of magnetization vector $\boldsymbol{M}$, γ_e is the gyromagnetic ratio, τ_1 is (spin-lattice) relaxation time for longitudinal and τ_2 is (spin-spin) relaxation time for transversal components of $\boldsymbol{M}$. Irradiating by microwaves is equivalent to applying of an oscillating field $\boldsymbol{B_1}$ that in the case of EPR, corresponds to the magnetic component of radiation. Adding the oscillating field into Bloch equations will result in

$$\frac{dM_x}{dt} = \gamma_e\left(B_0 M_y - B_1 M_z \sin \omega t\right) - \frac{M_x}{\tau_2}, \tag{17}$$

$$\frac{dM_y}{dt} = \gamma_e(B_1 M_z \cos \omega t - B M_x) - \frac{M_y}{\tau_2}, \tag{18}$$

$$\frac{dM_z}{dt} = \gamma_e(B_1 M_x \sin \omega t - B_1 M_x \cos \omega t) + \frac{M_z^0 - M_z}{\tau_1}, \tag{19}$$

where ω is an angular frequency of oscillating magnetic field B_1. A more detailed explanation of Bloch equations, the concept of a rotating frame which simplifies their notation as well as their steady-state solution can be found in literature [17, 21, 22].

1.2 General EPR instrumentation

Most EPR spectrometers operate in the X and Q microwave band region because they can simply use a conventional (resistive) electromagnet [23]. If the superconducting magnet is required, usually we are talking about a high frequency or high field (HFEPR)

spectrometer. They usually use microwave radiation in the W band or above. More information on HFEPR spectrometers is revealed in the second chapter.

The main parts of the CW-EPR spectrometer are: *Microwave bridge* that includes a microwave source, waveguides, circulator, resonance cavity, and detector. *Electromagnets* with their power supply unit (and cooling system), Tesla meter (or Gauss meter). Finally, a *modulation circuit* that significantly improves the signal-to-noise ratio (SNR) by using a lock-in amplifier for phase-sensitive detection (PSD).
Of course, experiments are usually controlled by a PC which also serves for processing, analysis, and storing of measured data [19].

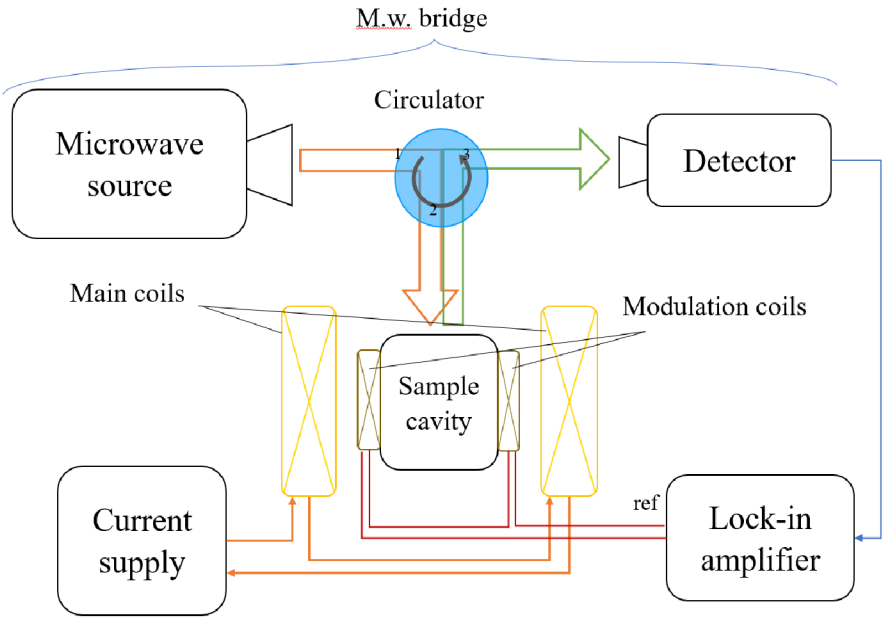

Figure 4: Functional diagram of ordinary continuous wave (CW) EPR spectrometer

Modern spectrometers mostly use microwave sources based on solid-state electronics such as YIG sphere, or impact ionization avalanche transit-time (IMPATT) diode [24], because of their small size, sufficient power, tunability, long life, and relatively low cost. Waveguides are essentially rectangular metal tubes that serve to deliver microwaves from the source to the resonance cavity with a sample [25]. A resonance cavity is usually just a metal box of cylindrical or rectangular shape in which the studied sample is placed. Resonance cavities are able to store microwave energy at a specific frequency, therefore no microwaves are reflected back. Along with resonance frequency, another important attribute of the cavity is quality factor Q which is expressed:

$$Q = \frac{2\pi \cdot (Energy\ stored)}{Energy\ disipated\ per\ cycle}\ [-] \qquad \text{or} \qquad Q = \frac{f_{res}}{\Delta f}\ [-]; \qquad (20)$$

where f_{res} is the resonance frequency and Δf is the bandwidth of the resonance cavity. Bandwidth can be easily estimated as a difference of frequencies at which reflected power decreases by half, or more exactly by -3 dB.

As the detector of microwaves usually a properly pre-biased Schottky diode is used. The diode converts the power of microwave radiation to current.[26].

An electromagnet may consist of a single solenoid, or can be made of two identical coils, whose distance is the same as their middle radius. This arrangement is called a Helmholtz coil (Figure 5), in which center there is a homogenous magnetic field. The power supply for the electromagnet has to be chosen concerning the parameters of the coils. The magnetic field is measured by a Teslameter with a Hall probe [19].

The last important piece in a CW-EPR spectrometer is a phase-sensitive detection (PSD) that significantly improves the quality of the EPR signal in terms of signal-to-noise ratio (SNR) compared to direct detection. An instrument that is used for PSD is called a lock-in amplifier. The basic principle of PSD in EPR is as follows: the magnetic field is slightly modulated by a sine signal at a reference frequency that is usually between 1–100 kHz. This signal is amplified in and brought to the modulation coil (another solenoid or Helmholtz coil).

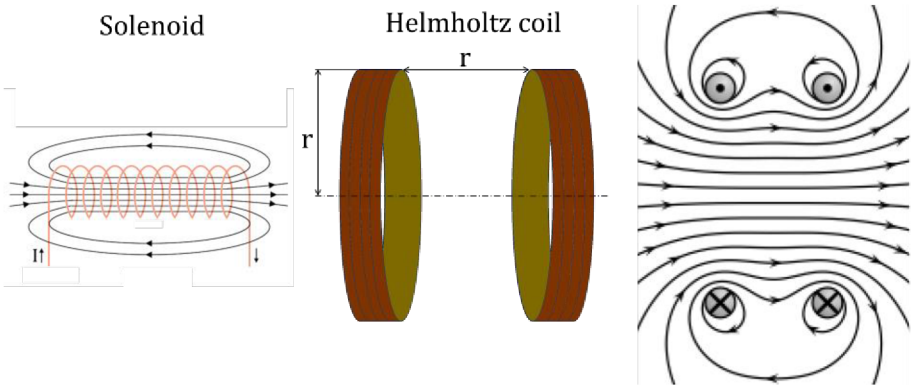

Figure 5: Solenoid (left) and Helmholtz coil (right) with homogenous magnetic field in its center. Distance between two coils equals their radius.

Applying modulation while sweeping of magnetic field will result in changes in reflected microwave power when absorption caused by EPR occurs. These changes will have the same frequency as the frequency of modulation. Detected microwave signal is brought to the lock-in amplifier, where it is mixed with the reference signal. Mixing of two harmonic signals will create two components. One frequency will be the sum of these signals' frequency and another of their difference. But, because the EPR signal has the same frequency as the reference signal, the second component will result in a DC signal with amplitude:

$$V_{psd} = \frac{1}{2} V_{sig} V_{ref} \cos(\varphi_{sig} - \varphi_{ref}). \tag{21}$$

Here V is a voltage amplitude, φ is a phase, suffix *sig* is used for the signal from detector and *ref* is used for the reference signal. In lock-in amplifier, this mixing is done twice. Second time is signal from detector mixed with 90° ($\pi/2$) shifted reference signal to prevent the case, when phase difference is zero. By applying a low pass filter, the higher frequency components are removed. If the two remaining DC signals are geometrically

summed, their result is a recovered EPR signal. In digital lock-in amplifiers, this signal is directly recorded and sent to a computer for processing into EPR spectrum [27].

1.3 Pulse EPR spectroscopy

Similarly, as in NMR, pulsed EPR experiments are currently preferred in the biological research field [28, 29]. They can decouple certain interactions to spotlight only desired ones which allows to access information that cannot be obtained by the CW-EPR. However, it is more expensive and technologically challenging. In some cases, the pulse EPR experiments can take longer than the CW-EPR. One of the capabilities of pulsed EPR is looking at spin systems via probing of spin-lattice (longitudinal) relaxation time τ_1 and spin-spin (transverse) relaxation time τ_2. The idea is to probe spin systems via their magnetization response to a short but strong microwave pulse (~10 ns, ~100 W). The pulse will excite transitions in a spin system at multiple resonance frequencies at once. The spin system then relaxes to equilibrium while generating a free induction decay (FID) signal (exponentially decaying oscillations of magnetization). In standard pulsed EPR measurements, sequences of pulses are applied and responses in the form of electron spin echoes (two mirrored FIDs) are recorded and usually Fourier-transformed into frequency spectra [30]. Various pulse sequences are summarized in Figure 6.

Electron-nuclear double resonance (ENDOR) clarifies hyperfine coupling of unpaired electrons with surrounding nuclei by stimulation of spin echo via pulses at EPR and NMR frequencies. Complementary method to ENDOR is electron-spin echo envelope modulation (ESEEM), which however uses only EPR pulses. The two-pulse method is simple and fast; however, the spectrum also contains the sum and difference of the basic nuclear frequencies [22]. Obtaining the spectrum by the three-pulse method is a bit more time-consuming, however, the spectrum is simpler and with narrower lines. Hyperfine Sublevel Correlation Spectroscopy (HYSCORE) is also called 2-dimensional ESEEM, in which two time intervals (t_1 and t_2) are varied [31, 32].

There is also a technique called pulsed electron-electron double resonance (PELDOR), also known as double electron-electron resonance (DEER), that excites two paramagnetic centers at different EPR frequencies and observes electron-electron spin-spin coupling [22]. Depending on a sample type, the PELDOR can be sensitive to distances up to about 10 nm, which makes it a suitable tool for studying of topology of large protein complexes.

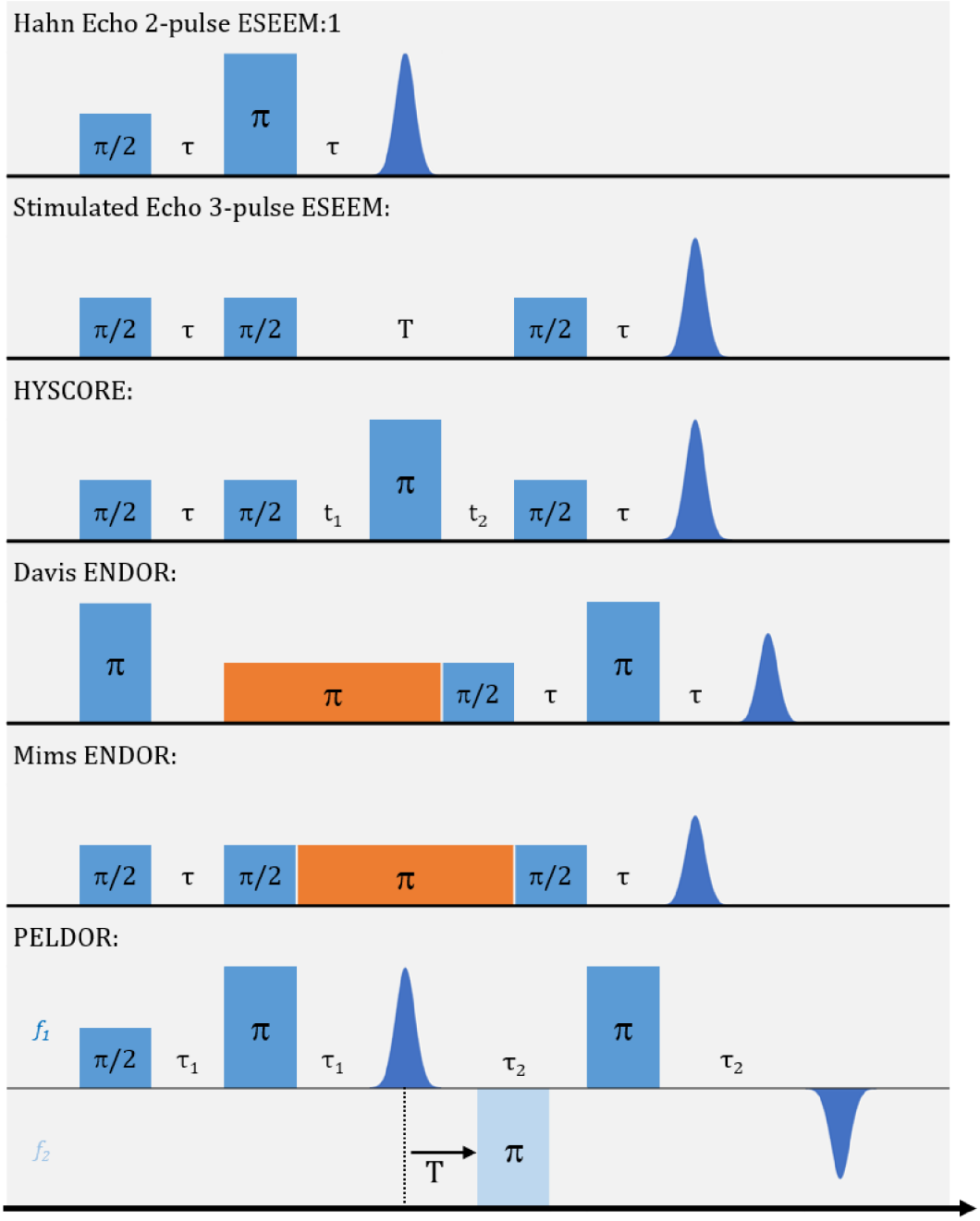

Figure 6: Pulse sequences of various type of experiments. Blue and orange color denotes microwave (EPR) and radio wave (NMR) pulses respectively. Inspired by [29]

Because of the technical obstacles, it is difficult to use pulsed EPR to quickly acquire a broad spectrum with a short dead time (<100 ns). Therefore, obtaining EPR spectra of paramagnetic species with very short spin relaxation time is challenging. Also, the acquisition of broader spectra is time-consuming because data has to be accumulated from repeated measurements. But that does not allow us to study fast chemical and biological processes. One way to overcome these limitations is using chirp pulses, which have broader excitation frequency spectra while keeping microwave power relatively low. Another way is to apply a rapid scan method described in the next section.

1.4 Rapid scan

Rapid-scan (RS) EPR is technique in which magnetic field or frequency of radiation is swept so fast that, time interval of a scan through spectral line is comparable to electron spin relaxation time. Generally, relation between sweep rate and relaxation time is:

$$\gamma\left(\frac{dB}{dt}\right) \geq \frac{1}{{\tau_2}^2} \quad or \quad \left(\frac{d\omega}{dt}\right) \geq \frac{1}{{\tau_2}^2}, \tag{22}$$

where a γ is gyromagnetic ratio, B is the applied magnetic field, ω is microwave angular frequency, and τ_2 is a spin-spin (transverse) relaxation time [33]. In such scans a passage effect appears which causes an induction response of the spin system that manifests to FID-like oscillations in detected signal (see Figure 7). However, these oscillations have an increasing frequency. In case of magnetic field scans, it is caused by continuously changing external magnetic field B_0 that affects the spin system and changes its precession (Larmore) frequency while it is decaying. In case of frequency scans, the frequency swept microwave signal is mixed with FID emitted by the spin system while Larmore frequency is constant. The rapid scan signal can be described by the convolution operation:

$$r(t) = s(t) * d(t) = \int_{-\infty}^{+\infty} s(\tau)d(t-\tau)d\tau, \tag{23}$$

or by multiplication in a Fourier space:

$$R(\omega) = FT|s(t)| \cdot FT|d(t)|, \tag{24}$$

where *FT* denotes Fourier transformation, *r(t)* is the rapid scan signal, *s(t)* is the FID signal, and *d(t)* is the driving function that describes the rapid scan excitation profile [33]. In order to recover the CW-EPR spectrum, the detected rapid scan signal must be deconvoluted. This is simply done in Fourier space as division. But, because in the field scan experiments Lamour frequency is not constant, the signal must be first transformed to reference frame by multiplication with the driving function before its Fourier transformation. A comprehensive derivation of solution for the rapid scan EPR deconvolution was described by Mark Tseytlin [34].

In addition, from the decay of rapid scan signal is possible to extract spin-spin relaxation time via fitting the measured spectrum to a spectrum simulated by modified Bloch equations expressed in rotating frame with B_1 field coordinate system {*u, v, z*}:

$$\begin{aligned} \frac{dM_u}{dt} &= -\frac{M_u}{T_2} - [\Delta\Omega + \omega(t)]\, M_v, \\ \frac{dM_v}{dt} &= [\Delta\Omega + \omega(t)]\, M_u - \frac{M_v}{T_2} - \gamma B_1 M_z, \\ \frac{dM_z}{dt} &= \frac{M_0}{T_1} + \gamma B_1 M_v - \frac{M_z}{T_1}, \end{aligned} \tag{25}$$

where M_u, M_v and M_z are projections of the total magnetization M_0, $\Delta\Omega$ is the offset of the resonance line from the canter of the sweep $\omega(t)$, and B_1 is the magnitude of the magnetic component of the microwaves [33].

In contrast to CW-EPR, in the rapid scan EPR experiments the phase sensitive detection is not applied, and a direct detection is used. Signal to noise ratio (SNR) is then improved simply by accumulating data from repeated experiments. Because scans are very fast (for example less than one millisecond) data accumulation from hundreds, or even thousands of scans can be collected in a fraction of second. Because the spin system is at resonance for a very short time, the rapid scan avoids saturation effect, and it is possible to use a higher microwave power for the further improvement.

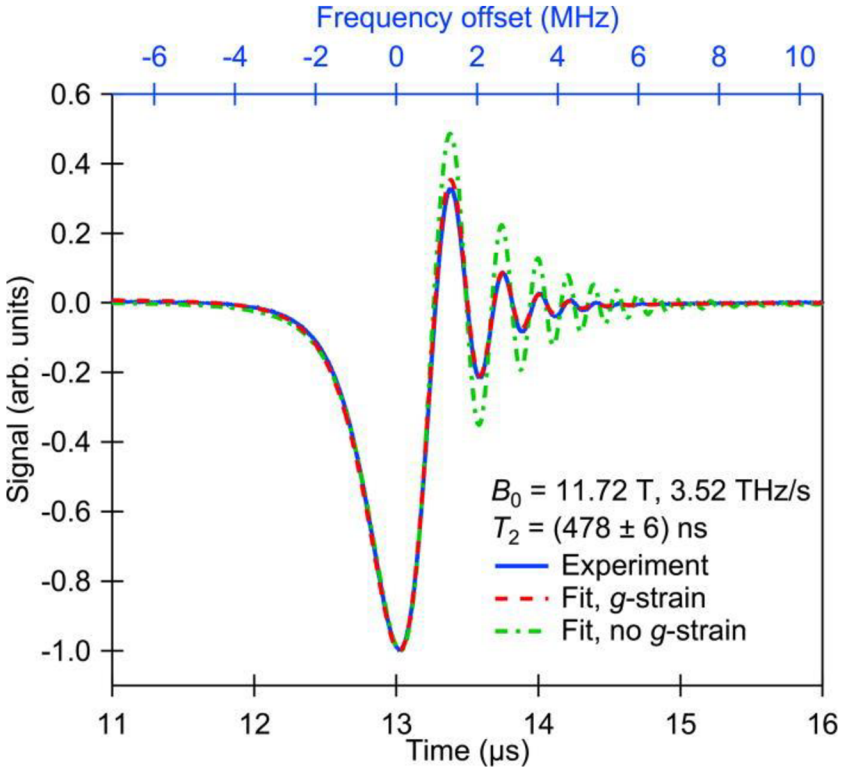

Figure 7: An example of frequency rapid scan ESR acquired on a single micro-crystal of lithium phthalocyanine (LiPc) fitted by simulation with homogeneous and inhomogeneous broadening models. Incident microwave power is 1 mW, 104 averages, and the total acquisition time is 5 s. Taken from [33].

A standard CW-EPR spectrometer that operates in L or S band can be relatively easily modified to operate in magnetic mode of rapid scan. Key is to achieve high tesla per second rate (time derivative of magnetic field). A triangular [16] or sinusoidal [35] scanning pattern can be used (Figure 8), but the later one is preferred for specimens with a short relaxation time, because it offers a higher ramp rate and is not that demanding to a driver that can simply excite the coil resonantly with a matching capacitor. It is recommended to use amplitude of alternating (scanning) magnetic field that is ten times larger than width of EPR spectrum. Resonance then occurs when magnetic field passes through quasi-linear area in middle of sine, where change of the field is the steepest. Signal is not acquired by a lock-in amplifier, but rather by instrument with a high

sampling rate and memory for accumulation of data such as oscilloscope. Fourier deconvolution is then used to recover slow-scan spectra.

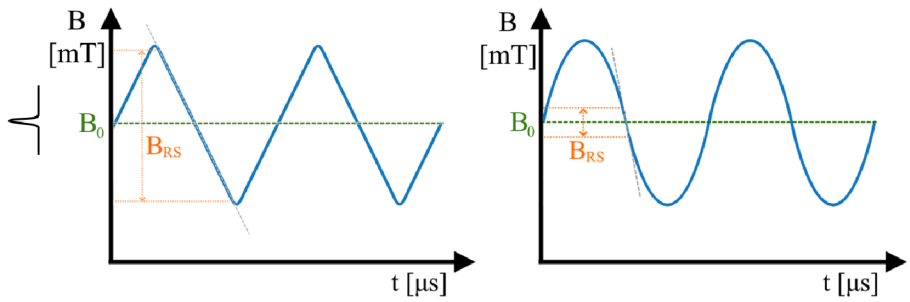

Figure 8: Comparison of triangular and sinusoidal scan profiles. B_0 is resonance field, and B_{RS} is a field range with quasilinear ramp rate.

In case of HFEPR is easier to scan frequency [33, 36] rather than magnetic field. Even though nowadays are available non-destructive pulsed magnets that could provide sufficient ramp rates [37, 38], their low repetition rate is limited by charging of capacitor banks, which can take several hours. However, modifying a HFEPR spectrometer for frequency rapid scan is not a trivial task, many obstacles can be avoided if this is included in requirements during a design of the spectrometer. In subchapter 3.5 there are further technical details describing upgrade of HFEPR spectrometer. Basically, the spectrometer has to operate in broad range. For this reason, waveguides are not as practical as a propagation through a free space via quasi-optics. Then a microwave source must allow fast frequency sweeps. Currently, is preferred arbitrary waveform generator. Then, a microwave detector must have a short response time, comparable to a spin-relaxation time. Because bolometers usually have a relatively slow response, they are replaced for example by a Schottky diode mixers. The arbitrary waveform generator makes possible to use a trapezoidal scan and acquire the rapid scan signal in area where driving function is constant (as it is shown on Figure 9). For this, the scan range must be comparable with linewidth and rising/falling time must be negligible to spin relaxation time. Then the rapid scan signal becomes an FID which processing is simpler.

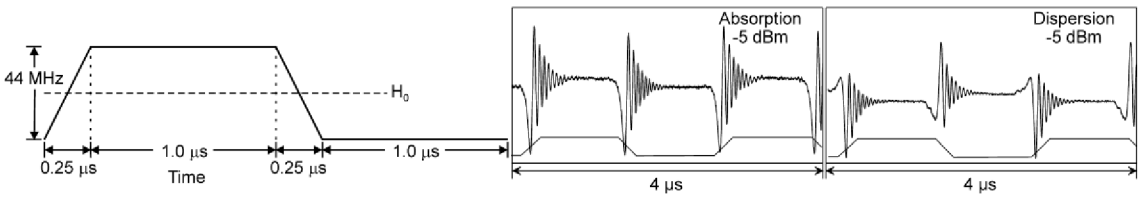

Figure 9: Trapezoidal driving function (left) and example of frequency rapid scan signal (right) of a 0.5mM TEMPONE sample. Taken from[36]. *The sweep rate is 176 THz/s, which is equivalent to 3.8 kT/s.*

1.5 Current software solutions for EPR spectroscopy

Companies such as Bruker BioSpin, JEOL and ADANI Systems (LINEV Group) that producers EPR spectrometers also software necessary for their operation and applications for simulation and evaluation of measured data.

To control EPR spectrometers, Bruker offers a few options. One that runs on Windows platform is WinEPR. It is designated to operate spectrometers of EMX series. Its module SimFonia is capable of simulating a CW-EPR spectra of solution and powder samples, thanks to a fast algorithm based on the perturbation theory. Other module SpinFit aids to identify radical adducts from a spin trapping experiments and can simulate and fit powder spectra. Results of simulation can be imported into SpinCount, which purpose is to determinate concentration and total number of spins in a sample.

A newer and more powerful solution for EMX spectrometers is Xenon software. This software package reflects a need for reliable and reproducible acquisition and processing of EPR data. It runs also on LINUX platform and integrates several modules including the SpinFit and SpinCount. Xenon has a sibling called Xepr that is designated for spectrometers of ELEXSYS series. Additionally, it supports pulsed operation of spectrometers [22, 39]. User interfaces of the Xeon and the Xepr are shown on the Figure 10 and on the **Chyba! Nenašiel sa žiaden zdroj odkazov.** respectively.

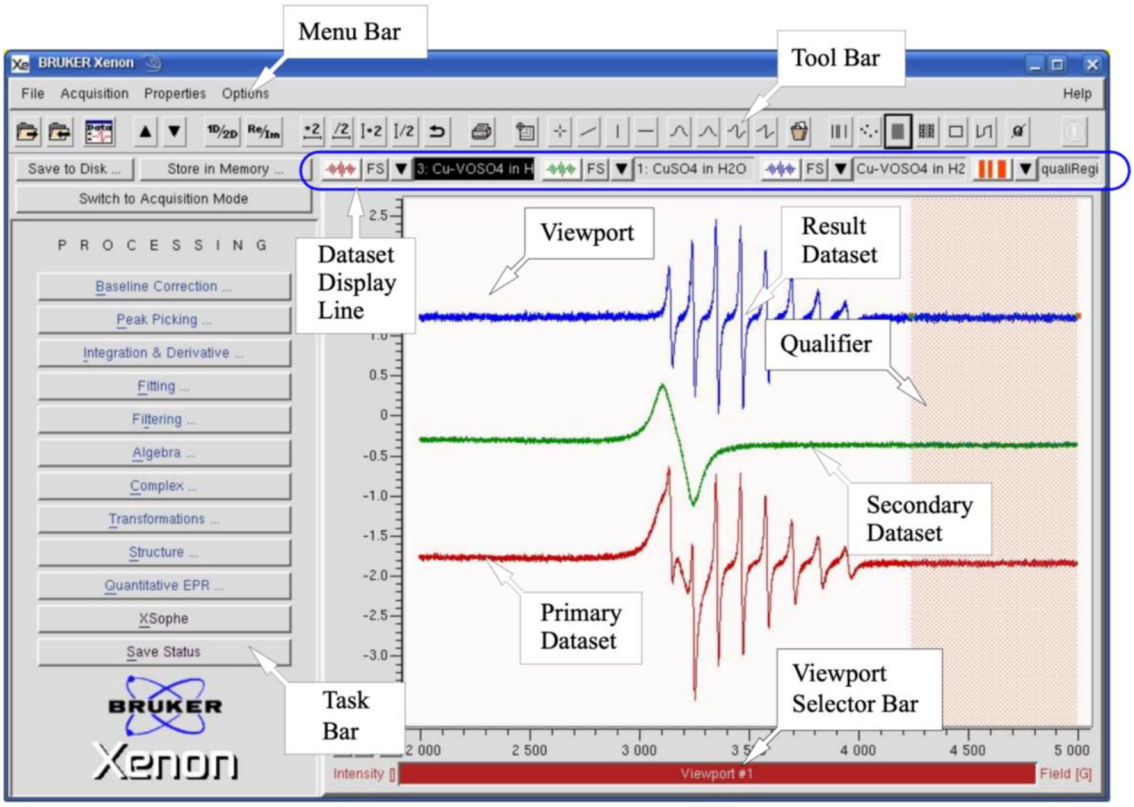

Figure 10: User interface of Xeon in processing mode. Taken from Xeon Data Processing Reference [40].

However, there are also alternative software solutions to control EPR spectrometers. One example is a SpecMan4EPR (Spectrometer manager) developed by a Boris Epel (FeMi Instruments, LLC) since 2002. It aims mainly to custom-made spectrometers that can include many optional hardware components. It was created in a development environment called C++ Builder. SpecMan4EPR is based on a Client-Server architecture. The server is responsible for execution of code that manages a hardware. The client on the other hand just provides a graphical user interface (GUI) to control experiment.

Currently it is capable to execute experiments for CW and pulsed EPR, ENDOR, ELDOR, ESEEM and dynamic nuclear polarization (DNP) [41, 42].

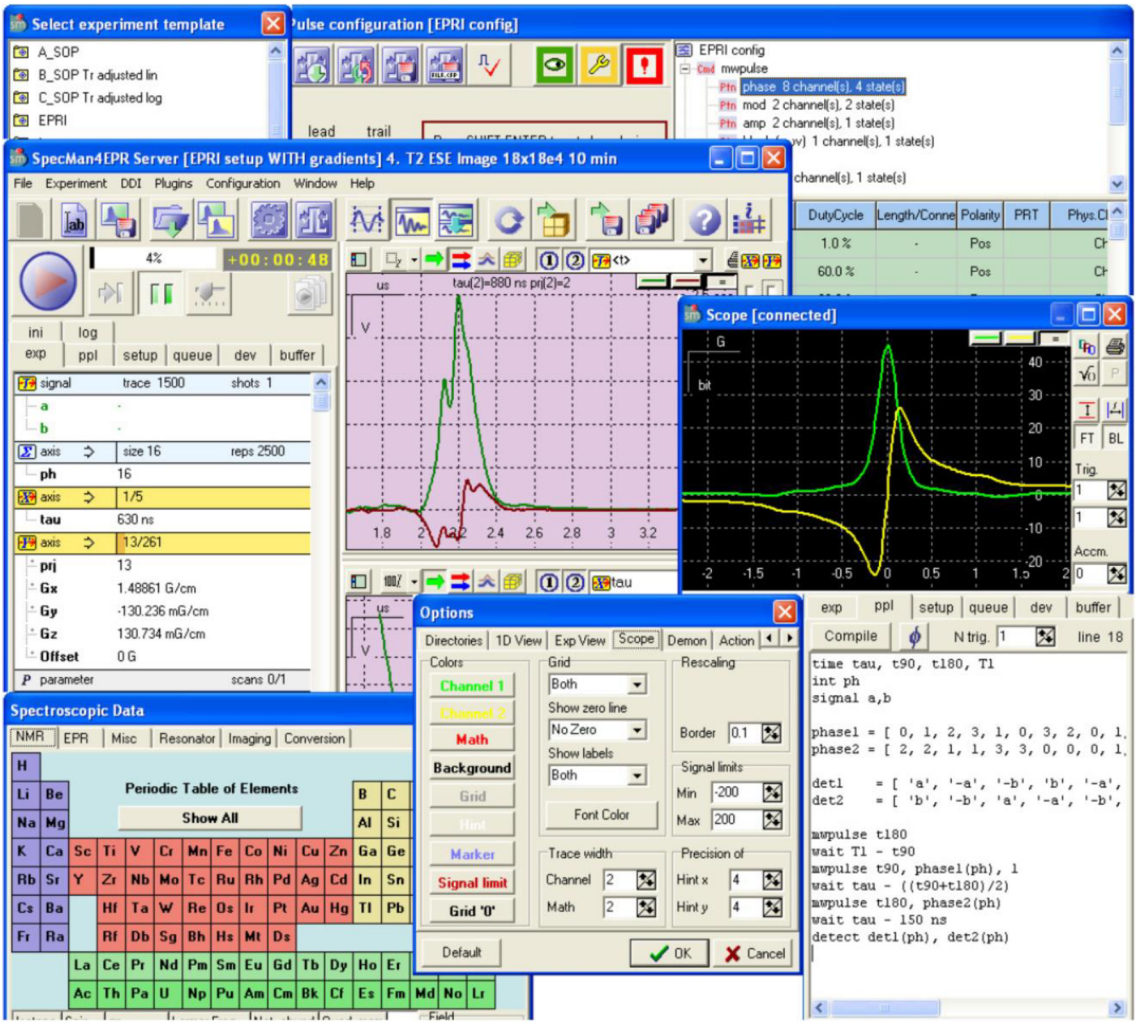

Figure 11: Various windows of SpecMan4EPR GUI. Taken from poster of Boris Epel and Reef Morse [41].

One of the most used freeware software for EPR spectroscopy is an EasySpin. It is a comprehensive MATLAB toolbox for simulating and fitting of EPR spectra [43, 44]. This computational EPR package uses concept of the Spin Hamiltonian for simulating of various EPR spectra. It contains several core functions that can be combined to create a flexible simulation for various cases. It also has a high-level function for the CW-EPR spectra simulations of liquid, an isotropic and anisotropic solid state samples, and also the CW and pulse ENDOR spectra. The EasySpin can also load spectra measured by Bruker spectrometers and fit them by varying parameters of the simulated spin system.

2 Equipment for HFEPR spectroscopy

To investigate materials containing more paramagnetic species that have similar *g*-factor, instruments (EPR spectrometers) with a higher spectral resolution are required. A simple approach to this is to go for a higher excitation frequency. EPR spectroscopy that is done with excitation frequencies above 90 GHz (W-band) or in the magnetic field that exceeds 3 T is usually considered to be a high-field/high-frequency EPR (HFEPR).

2.1 Electromagnets and superconducting magnets

In HFEPR the superconducting magnets are used to create high magnetic field. A coil of the magnet has to be designed to stay within superconducting state in a full range of required magnetic fields [45]. The coil is placed in a cryostat to be cooled by a liquid helium. A simple diagram of the cryostat is drawn in Figure 12. Because price of helium is rising (about 20-35 USD in 2020) [46] and not all facilities have built the recovery line infrastructure, some cryostats use a so-called cryogen-free system. The helium circulates between the cryostat and the compressor, while it is continuously liquefied [47, 48]. Cryogen-free systems adds acoustic noise and mechanical vibrations.

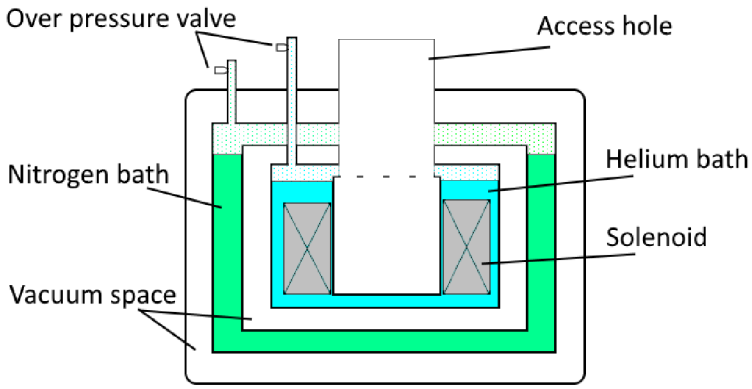

Figure 12:A diagram of a cryostat for a superconducting magnet.

Large inductance of superconducting magnets limits their charging speed. Superconducting wires are coated with a thin layer of copper to keep some degree of conductivity in case of a sudden loss of superconductivity known as a quench. During the quench energy stored in the magnet is dissipated in the form of heat. That leads to sudden evaporation of helium, and consequently overpressure in the cryostat. In addition, the coil is under sudden mechanical stress and the voltage on its terminals will rise in response to rapid change of the current. [45]. Magnet and its power supply have a passive and active protections that helps to dissipate the excess energy and prevents overvoltage. The superconducting magnets can be equipped with a superconducting switch. It allows to set the magnet into persistent mode in which the magnetic field remains constant even if the power supply is disconnected [45].

2.2 Millimeter and submillimeter wave sources

Although nowadays there are many different kinds of microwave and infra-red sources, it is very challenging to create a powerful, compact, tunable, and stable source with narrow band output in the range of one decade below and above 1 THz, so this region is known as a terahertz gap (see Figure 13). Whereas in the terahertz gap region can be found many rotational and vibrational frequencies of molecules, it attracted the attention to develop spectroscopic and imaging applications in fields such as astronomy, biomedical diagnosis, security, and chemical analysis. This development was possible thanks to the simultaneous advances in terahertz technology [49]. However, not all currently available sources are suitable for all applications in HFEPR spectroscopy. This section contains a brief overview of suitable millimeter and submillimeter microwave sources. More information can be found in the literature [24].

An oscillator based on impact ionization avalanche transit time diode (IMPATT) are used in pulsed HFEPR for frequencies up to ~400 GHz. For applications that require high power, a gyrotron might be the first suitable choice. In 2001 a gyrotron with an output power of 100 W at frequency 460 GHz was built at MIT [50]. Currently are popular solid state sources containing microwave multipliers combined with amplifiers. These devices consist of nonlinear circuits that cause distortions of input signal. Consequently, higher harmonic frequencies are produced, and the bandpass filter selects only a desired harmonic and suppresses other harmonics as well as the fundamental frequency. As nonlinear device can be used GaAs Schottky diode, heterostructure barrier varactor (HBV) also known as varicap, or a high electron mobility transistor (HEMT). [51, 52].

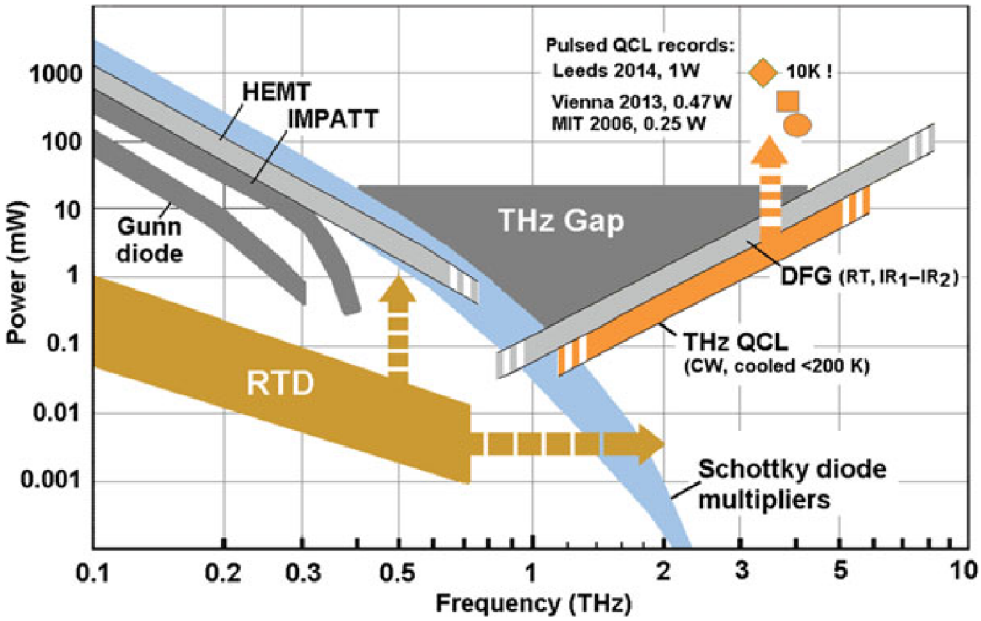

Figure 13: Overview of solid-state THz sources in 2017. Taken from [49]

2.3 Detectors in Terahertz region

The Schottky diodes can also be used in EPR as detectors of electromagnetic radiation at terahertz frequencies. They have a good responsivity (<1μs) at room temperature for radiation even above 0.6 THz. Modern processes allow creation of structures with a very high cut-off frequency of up to 4.4 THz [53]. They suffer mainly from thermal noise, and because most EPR measurements deal with a low signal, techniques that suppress the noise have to be applied. Usually a heterodyne detection is used, in which the diode serves also as a mixer. At the output of the detector is therefore a signal of intermediate frequency. This signal is usually amplified by a low-noise amplifier [54].

Another commonly used type of detector for THz radiation is bolometer. They are mainly used in astronomy because of their unrivaled sensitivity, relatively low noise-equivalent power (NEP), and wide frequency range (0.15–20 THz). The working principle of bolometers is in the heating of the sensing element by incident radiation, which leads to a change in its resistance. The main drawback of bolometers is their relatively slow response, which depends on the heat capacity of the sensing element. Another disadvantage is that they have to operate at cryogenic temperatures of around 4 K, thus needing to be cooled by liquid helium. For example, the fastest InSb hot electron bolometers cooled by liquid helium have an electrical sensitivity >4V/mW, NEP below 800pW/√Hz, frequency response up to 600 kHz, and bandwidth of 60–1500 GHz [55]. They can be also used as a mixer for homodyne detection and therefore are suitable for a CW-HFEPR [54]. Development of new graphene-based bolometers is currently in progress and can lead to even faster and more sensitive detectors [56].

2.4 Quasi optics

Because microwaves above 100 GHz have a corresponding wavelength below 3 mm, it becomes difficult to fabricate along waveguides suitable for higher frequencies. They would also have considerable losses. It is more convenient to use quasi-optical (QO) components and propagate mm and sub-mm waves as a Gaussian beam [25, 54, 57]. The only necessary waveguides in HFEPR are corrugated feedhorns. They are used to transmit a Gaussian beam from the microwave source into free space and collect the beam from free space into a detector [48, 58].

An elliptical mirror (made of good electric conductors) [59] and dielectric lens (usually made of PTFE [60]) are used to refocus the beam. A wire-grid polarizer reflects waves with electrical component parallel to wires, while those that are perpendicular can pass through its grid structure. A Faraday rotator is made of hard ferrite whose magnetic field is aligned along the axis of the beam propagation, causing a rotation of polarization. The wire grid polarizers and faraday rotators can be used to create a broadband QO circulator [57].

3 FRaScan HFEPR spectrometer

This chapter introduces the HFEPR FRaScan spectrometer built in the EPR laboratory at the CEITEC BUT. The spectrometer was designed mainly to utilize a Frequency rapid-scan method (development was supported by ERC Starting grant AN714850), but it is also capable of CW-EPR, and frequency swept (FS-EPR) measurements. Another advantage of the spectrometer is in variety of samples that can be studied thanks to a rich palette of developed sample holders [61, 62]. At last, a software solution for computer-controlled experiments was developed in LabVIEW [63, 64]. A brief description of the spectrometer is given in this chapter.

3.1 Description of spectrometer

The spectrometer was built from parts supplied by different companies. A cryogenic system from Cryogenic Limited includes a cryogen-free superconducting magnet (CFM) whose maximum achievable magnetic field is 16 T, and variable temperature insertion (VTI) subsystem to regulate the temperature of a sample space in the range from 2 to 325 K. Another important part of the spectrometer are microwave sources (synthesizers with amplification-multiplication chain) and detectors (Schottky diode mixers), which were bought from Virginia Diodes Incorporated. To propagate microwaves from sources to samples and then to detectors a quasi-optical setup that covers a frequency range of 80 – 1100 GHz was manufactured by Thomas Keating Limited. To implement the PSD, a middle-frequency lock-in amplifier (MFLI) from Zurich Instruments AG was used. Most parts of mechanical construction (for example strut profiles and servo motors) were supplied by Bosch Rexroth AG.

The cryogen free system is using pair of compressors (Sumitomo F-70H) and a pair of pulse tube cryocoolers (Sumitomo RP 082). The cryostat serves as a thermally isolated case for the magnet. A temperature monitor model 218 (Lake Shore Cryotronics, Inc.) tracks temperatures at functional parts of the CFM system. It is connected to a PC via a serial port. The cryostat, the cryocoolers, and the temperature monitor are labeled in Figure 14. The CFM is powered by SMS120C power supply with a reversing switch option that can change the direction of electric current to make the magnetic field of negative polarity. The SMS120C is backed-up via uninterruptible power supply (UPS) Sentinel Pro (from RPS Spa - Riello Elettronica Group). The CFM also has a superconducting shunt (switch) for switching between a ramping and a persistent mode of operation by heating (and cooling) the shunt above (and below) a critical temperature. A heater of the shunt is powered via an auxiliary output of SMS120C.

The VTI subsystem is crucial for temperature dependency measurements. It uses a secondary cooling circuit to adjust the temperature in a sample space (VTI bore). The secondary circuit is thermally coupled with the primary cooling circuit that provides

sufficient cooling power for liquification of the helium before it is exhausted into the sample space. A heater and a temperature sensor are placed at the exhaust of helium into the sample space. Both are connected to a Model 350 Temperature controller, which regulates the heating. The VTI bore is sealed on its top with a gate valve. An airlock on top of the gate valve enables the insertion of an EPR probe without exposing the VTI subsystem to air contamination. The airlock is evacuated by a scroll pump. The scroll pump, the airlock, the EPR probe, and the temperature controller are labelled in Figure 14.

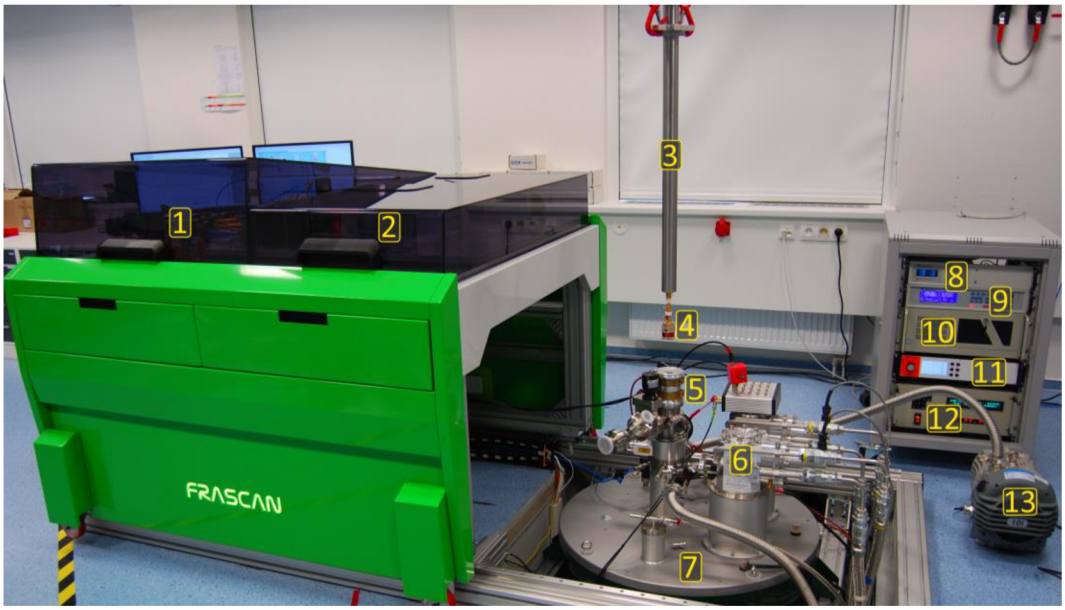

Figure 14: HFEPR FRaScan spectrometer. 1) Cover above terahertz sources, 2) Cover above QO components, 3) EPR probe, 4) Sample holder, 5) Airlock, 6) Cryocooler head, 7) Cryostat of CFM, 8) Temperature monitor, 9) Temperature controller, 10) PC, 11) Piezo-controller, 12) Power supply for CFM, 13) Scroll pump for Airlock.

The spectrometer implements a heterodyne detection technique to receive EPR signals from terahertz waves. For this purpose, it has a pair of terahertz wave sources, which can be seen in Figure 15. One generates a wave for the excitation of the sample (RF) and another one serves as a local oscillator (LO). Both sources consist of a microwave synthesizer and amplification and multiplication chain (AMC) with an input range of 9 – 14 GHz. Additional doublers and triplers can be used to cover the range 82 – 1020 GHz via several subsequent subranges. The LO synthesizer is locked to the RF synthesizer and generates a signal whose frequency is lifted by the desired intermediate frequency (IF) portion (divided by multiplication factor). Then even when RF synthesizers generate frequency-swept signals, the IF is kept constant. To control output power a pair of adjustable attenuators is attached to feedhorns from which both terahertz waves are transmitted to the quasi-optical system.

In the quasi-optical (QO) system, the wave generated by the RF source is first guided to a circulator made of several polarizers and a Faraday rotator. Then it passes through a window on top of the EPR probe head, where it enters a corrugated waveguide. The wave

propagates further through a waveguide in a sample holder passes through a sample, reflects from a mirror, and on the way back passes again through the sample. As the wave interacts with the sample (is absorbed), the polarization of the wave changes. Then in the circulator, a component of the same polarization as the original wave is directed to a reference (co-polar) mixer. On the other hand, the component of different polarization is diverted to the measuring (cross-polar) mixer. In the case of the wave from the LO source, the situation is much simpler. The wave is split on a wire grid polarizer and one component is directed to the reference mixer and the other component is directed to the measuring mixer. The QO setup was designed to match the distance of both LO pathways and both pathways of the wave that returns from the probe. The distance matching ensures that waves hit the detectors with the same phase. Signals at an intermediate frequency from both detectors are amplified and brought into another down-converting mixer. The resulting signal is then brought to a high-speed digitizer in case of FRaScan experiments or into a Lock-in amplifier in case of CW-EPR and FS-EPR experiments. A top view of the QO system is in Figure 15. Additional information on the QO system can be found in the thesis of Antonin Sojka [65]. Even though the QO system is passive, its coupling to the waveguide of the EPR probe is crucial. The coupling is adjusted via precise positioning of the QO table by servomotors.

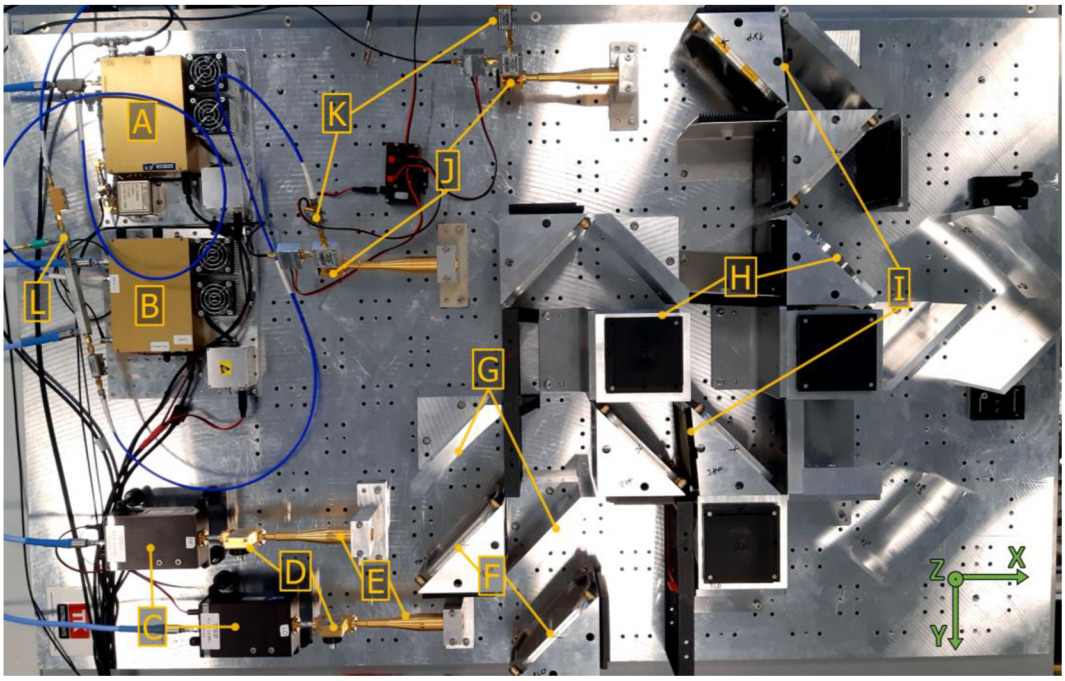

Figure 15: Terahertz system. A) Main synthesizer, B) Following synthesizer, C) AMCs, D) Attenuators, E) Feed horns, F) Polarization grids, G) Focusing mirrors, H) Adjustable polarizers, I) Faraday rotators, J) Terahertz mixers, K) Microwave amplifiers L) Microwave mixer

In CW-EPR and FS-EPR experiments a modulation of EPR signal via low frequency (~1 kHz) magnetic field, and later demodulation of detected signal in a lock-in amplifier is used to improve a signal-to-noise ratio. Theoretical basics for this approach can be found in the Chapter 1.2. A higher modulation frequency (>10 kHz) can be achieved by connecting a resonance capacitor in series with a modulation coil wind up on a sample

holder. However, at higher frequencies, an eddy current induced in the waveguide suppresses and deforms the alternating magnetic field around a sample. The digitized and demodulated EPR signal is transferred, to a PC. In the case of Frequency Rapid-Scan (FRaScan) measurements, the modulation is not used, but the signal is enhanced by many accumulations from repeated scans. For this, the data are acquired via digitizer ADQ7 from Teledyne SP Devices. To remove a background, the coil on the sample holder can be driven by a positive and negative direct electrical current from the source meter unit, that would lift the magnetic field in and out of resonance. However, this can be done only in a limited range of current, that the coil can withstand.

The servomotors that control the position of the QO table are driven by five IndraDrive compact converters HCS01. The converters are supplied via a secondary switchboard that contains a 100mA residual-current device, EMC filter, 24V DC power supply for the converters, and timer relay that delays a 230V AC supply for Y- and Z-axis converters by one second to reduce a current spike. Servomotors are equipped with a brake that prevents unwanted movement and an encoder with a battery that prevents loss of actual position. The converters are connected with a PC via an ethernet chain, that starts with an X-axis converter. For safe operation, the maximum limits for speed, acceleration, torque, and position were set and are controlled by the firmware of the converters.

3.2 EPR probes and sample holders

The role of an EPR probe is to place a sample holder with a sample in the center of the magnetic field and bring the terahertz waves there. A waveguide is commonly used to transmit the terahertz waves in restricted space. It is a central part of the EPR probe. It must be made of well-electrically conductive material for good transmitting properties and at the same time a poor thermal conductor to minimize a transfer of heat from the outside of the cryostat into the sample holder. For the FRaScan HFEPR spectrometer two corrugated cylindrical oversized waveguides were made by Thomas Keating Ltd. from alpaca (aka German silver), one optimized for a lower frequency of about 110 GHz and the second one optimized for a higher frequency of about 420 GHz. Each waveguide is equipped with a feed horn at the bottom and mounted to a probe head on its top. The feed horn makes an interface between the waveguide of the EPR probe and the waveguide of a sample holder. The probe head provides a mechanical fastening of the waveguide. It also has several ports to hermetic connectors for electrical signals (Fischer Connectors SA), and a Mylar window for the terahertz waves.

A set of sample holders was fabricated to cover a variety of sample forms (powder, crystal, liquid, electronic devices, air sensitive). All sample holders implement the common bayonet mounting mechanism, have the same outer diameter and connectors for

electrical signals, and are designed to keep the same position of a sample relative to the superconducting magnet. [61].

The first made sample holder was a simple sample holder (SSH) which is shown in Figure 16. It is used for solid-state samples such as crystals, or powders. Compared to other sample holders the SSH is the most robust and carries the modulation coil with the highest inductance and field-to-current ratio. To study the anisotropic properties of crystal samples, a rotating sample holder (RSH) was made by implementing a piezoelectric rotator ANRv51 from Attocube Systems AG. As can be seen in Figure 16, the piezo rotator is mounted on a base platform of the RSH.

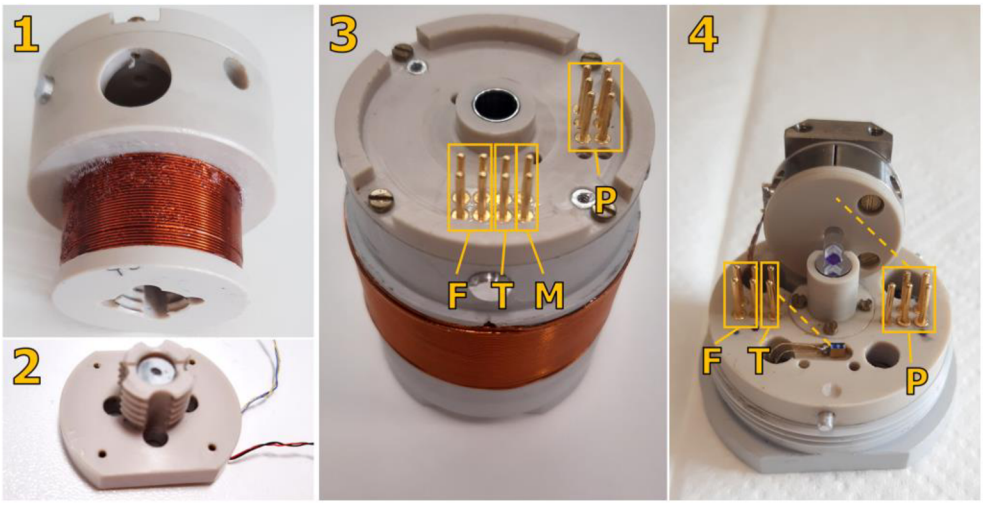

Figure 16: Sample holders. 1) Body of the SSH, 2) Base of the SSH with mirror and sample, 3) Body of the RSH (pins: F- for magnetic field sensor, T- for the temperature sensor, P- to piezo rotator), 4) Base of RSH with a sapphire rod.

By a simple modification of the SSH, a liquid sample holder (LSH) was made. This sample holder contains a sapphire window which hermetically seals a liquid sample, to prevent its evaporation due to a low pressure.

The chip-sample holder (ChSH) is dedicated to electron-transport measurements. It can use up to 16 pins for the connection of electronic devices (transistors, bolometers, solar cells) to measure their properties at low temperatures, high magnetic fields, and under microwave irradiation [66, 67]. Then there is a carousel sample holder (CSH) in which up to 6 samples can be loaded at once. This saves the time needed for change of the samples (hours for a low temperature). So far mentioned sample holders were also reported in publication of Antonin Sojka [61]. There is also one sample holder made by Artur Solodovnyk for electrically detected magnetic resonance (EDMR) measurements [62]. This method allows to detection of even a small quantity of dopants or impurities. The EDMR sample holder is also equipped with optical components for light excitation.

3.3 Modes of operation

The spectrometer utilizes several types of EPR measurement methods. The simplest one is a CW-EPR (theory in chapter 1.2.). In this mode, main synthesizer operates at constant frequency in a selected range and magnetic field is ramped from starting value till the end value at desired ramp rate. Because power supply has a reversing switch, it can also ramp through a negative magnetic field as well. A ramp rate is usually set in range 0.5 to 3 mT/s. The limiting factor is mainly residual heat created during the charging of the magnet, and this heat has to be balanced by the cooling power of the cryocoolers. The frequency range of microwaves is constrained by a set of terahertz components (AMCs, multipliers, feedhorns, faraday rotators, and mixers) that can be exchanged if needed. Because each set has relatively broad operating range, measurements can be easily repeated for a several frequencies without any manual action of operator. This is useful for example to distinguish EPR lines of paramagnetic centers that have a different g-factor. For a good experimental result, it is crucial to choose an appropriate setting of lock-in amplifier, specifically modulation frequency, modulation amplitude, and a time constant (or a cutoff frequency) of a low pass filter. To do this, one must consider an expected width of lines, their intensity, and the ramp rate of the magnetic field. Modulation amplitude should be about a quarter of line width. The time constant should be ten times lower than scan time through the EPR line [18]. A higher modulation frequency should generally lead to a higher sensitivity, but it can also distort lines. An eddy currents induced in a waveguide may lead to heating and inhibit a modulating field to penetrate to a sample (skin effect). The modulation frequency between 1–20 kHz was empirically found as suitable in this setup. Using of CW-EPR method is the most time demanding, but is also reliable, easy to use, and brings good results in terms of signal-to-noise ratio.

Another type of measurement that can be done with the spectrometer is frequency-swept EPR (FS-EPR). This method contrasts with the previous one in the sense that now the magnet is set to persistent mode which keeps the field constant, while the frequency of microwaves is swept. A sweep rate is no longer limited by the induction of the magnet; therefore, a single scan can be done in about one second. On the other hand, it usually works well only in a narrow frequency range (<1 GHz). In a broader span, several effects ruin the quality of results. The most significant are standing waves, caused by unwanted reflection of microwaves at quasi-optical components. Because scans are fast a time constant has to be much smaller than in CW-EPR and the modulation frequency needs to be higher. A signal-to-noise ratio can be improved by an accumulation of data from several scans. The effect of standing waves can be suppressed by subtraction of the background obtained by measuring at different magnetic fields. The FS-EPR mode is mostly used for samples in which the EPR signal gives narrow and intense lines. It can be also used in cases when distortion of lines is acceptable. One example of its practical

use is searching for optimal alignment of the quasi-optical table. Because a single scan is done within one second, the intensity of an EPR signal can be evaluated while servo drives move the table to another position.

By combining of previous two approaches, it is possible to obtain the so-called Zeeman diagram. Simply, several hundred (or thousand) frequency scans are done during a single scan of the magnetic field. Data from such an experiment shows how a microwave frequency that excites a spin transition depends on a magnetic field. Because in this case, a partial corruption of EPR lines is acceptable, frequency scans can be about 10 GHz broad, and a field scan can be a few Teslas wide. By repeating measurements in another neighboring frequency ranges, an obtained data can be concatenated to create a large-scale Zeeman diagram. Moreover, CW-EPR spectra of sufficient quality can be extracted for any frequency (shown later in the Figure 27).

3.4 Software solution

For an effective use of all the spectrometer's components, a custom software solution was developed. It was an integral piece for a practical part of this thesis. To speed up the software development process a LabVIEW was used to implement CW-EPR, FS-EPR, and a two-dimensional (2D-EPR) mapping (Zeeman diagram) measurement. These three programs were grouped in a main software solution which is described in this section. For frequency rapid-scan measurements only a prototype of software was developed in MATLAB so far. Implementation in LabVIEW is subject to further extension, however, missing native support for an essential digitizer card makes it challenging. In this chapter brief information about software solution will be provided.

An object-oriented design was partially applied in the main software solution. In this sense software solution was split into modules to encapsulate code of related tasks. For example, modules that will be further referred to as submodules, are responsible for remote control over hardware subsystems of the spectrometer such as magnet, microwave sources, VTI, lock-in amplifier (later also for field sensor, sample rotator, and carousel). These submodules operate above an instrument driver as a higher abstraction layer and can be reused and optionally modified in projects that require control over the same instruments. Each module implements a queued message handler (QMH) design pattern. It is a well well-known design pattern for LabVIEW applications [68, 69] and is also a backbone in popular framework Delacor Queued Message Handler (DQMH) [70]. The QMH uses a queue (FIFO buffer) to exchange messages between parts of the program which runs asynchronously (in other threads). This allows submodules to run independently of each other, and exchange status properties or receive commands from a commanding (or supervising) module. To generalize the exchange of messages among modules, a variant datatype was used as a basic element for queues. The variant is a datatype specific for LabVIEW and can be used as a universal data container for a

complex datatype such as nested structures. Each instrument controlling submodule waits till a message occurs in the incoming queue. The message is then converted from a variant into a structure specific to the module (example shown in Figure 17) which contains a command in the form of Enum and data in the form of a variant. If the command is valid, the module further converts the variant with data into an appropriate datatype (bool, double, string, array, structure) and executes the required action. The action can be for example a setting of a new parameter value or obtaining some data from an instrument. After successful execution, a response message is sent to an outgoing queue, and the module waits for another message.

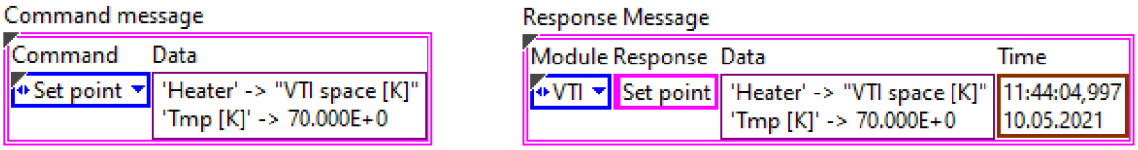

Figure 17: Structure of message clusters. At left is message containing a command for the VTI control module, at right is a message after successful execution of requested action.

Further submodules were developed to enable the basic functionality of the spectrometer:

A magnet module controls cryogen free magnet (CFM) subsystem that is responsible for setting of static external magnetic field in the sample area at the desired ramp rate. For the basic operation of CFM, control over the power supply unit (PSU) and the temperature monitor is necessary. *The temperature controller module* manages the operations of the temperature controller that adjusts the temperature of helium in the VTI circuit (secondary cryostat). It can also control a heater in a sample holder when it is connected. *Terahertz source module* controls both microwave synthesizers. The submodule gets a single data cluster that contains all parameters for setting the synthesizers: start frequency, end frequency (is ignored in CW measurements), sweep time (is 0 in CW measurements), and an offset frequency that projects into an intermediate frequency between *terahertz sources*. A frequency multiplication factor has to be taken into account in the higher software layer (supervising or commanding module). *The Lock-in module is dedicated to control the MFLI* for the modulation and demodulation of the EPR signal. The demodulator's data can be read point-by-point every 100 ms (in CW experiments), or as a set of data points (in FS-EPR and 2D-EPR mapping). The module was extended to measure the electrical current that runs through the modulation coil by multimeter, for accurate setting of modulation amplitude. The s*ervo drive module* controls the movement of the QO system in all three axes X, Y, and Z. *The rotator module* controls the piezo rotator driver for setting the orientation of crystal samples. S*ource-meter module* is mostly used to drive a hall sensor to measure the actual magnetic field but can be also used to measure the I–V curve of electronic elements sensitive to microwaves.

Further instrument submodules are planned to extend functionalities of the software: *Power monitor* to monitor the status of UPS. *PiezoMotor controller* that would

allow full integration of carousel sample holder. Development of a LabVIEW driver is in progress, and subsequent implementation of the submodule should be then trivial. *Digitizer module* to integrate the acquisition of rapid-scan signal *and Waveform generator module* to generate arbitrary waveforms.

For each subsystem control module, a simple prototype of supervising (commanding) module was made, just to test its functionality. The supervising module was based on a design pattern combination of a state machine (SM) and event handler.

By derivation from the supervising module, three commanding modules were made, one for each type of measurement (CW-EPR, FS-EPR, and a 2D-EPR mapping). Unlike simple supervising modules, they are able to manage multiple instrument control modules and contain execution logic for measurement routines. A state in which the queue of incoming messages is handled contains a further case structure dedicated to managing various instrument control modules. Also, a code for a state that handles user actions is more complex because GUI contains a large number of elements. The GUI of a program is divided by a tab control, into several parts for a different purpose.

The *Status* tab displays the status of connected instruments. The *Adjustment* serves to directly control individual parameters and actions of instruments. It contains clusters with control elements for the superconducting magnet, microwave sources, servo motors of the quasi-optical table, the lock-in amplifier, temperature controller, sample piezo-rotator (goniometer), and source meter unit. The *Measurement* tab shown in Figure 18 used the most. It contains options to set, measurements via an automation script, which is made as an array of clusters. A *Run script* button triggers an automated measurement sequence. The data file of CW measurement is a text file that has a header part and a data part, separated by a single line of underscores. This format was chosen because it can be opened even with a basic text editor and the data can be simply imported into any data analysis software. Depending on the magnetic field range and ramp rate, the size of the file is typically about 1 to 10 MB. When a particular measurement is done, the data file is closed and next executable line is selected and the procedure automatically repeats, until there are no more executable lines in the script. The script can be also loaded from another tab called a *Script editor.* The *Script editor* tab is intended to manipulate the script for automated measurements (generate, modify, save, and load). The operator can load a script from the *Measurement tab* and edit it manually. The current script can be saved as a structured text file and later loaded in the *Script editor.* .In the *Measurement review* tab data from finished measurements can be displayed, reviewed, and compared. The last *About* tab contains only basic information about the program and a brief guide for using it.

Figure 18: GUI of main program for CW-EPR measurements. On the top-left are controls to specify data file path. At the bottom part is a measurement script for automated batch of measurements.

The other two commanding modules (for the FS-EPR and the 2D-EPR mapping), have a similar GUI as the one for CW-EPR. The main difference is in the *Measurement tab* (Figure 19 and Figure 20).

The FS-EPR and 2D-EPR mapping can easily create large datasets (about 100 MB collected in a minute). Storing data in a text format would not be efficient anymore, therefore the NI TDMS (technical data management streaming) file format was used [71].

Figure 19: GUI of controlling module for FS-EPR measurements.

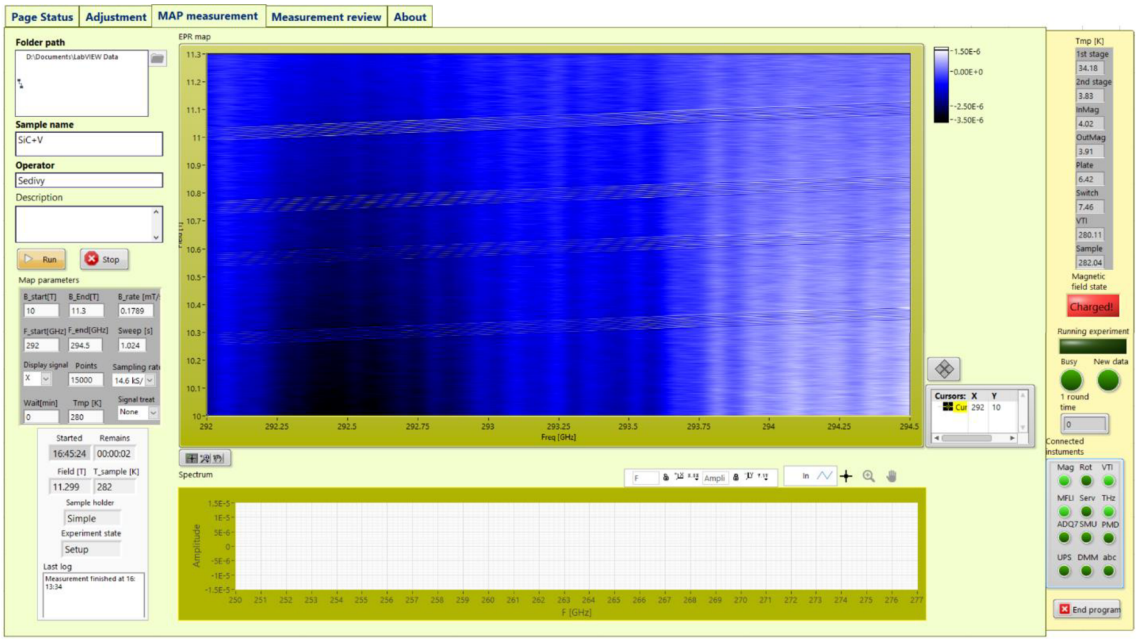

Figure 20:GUI of controlling module for 2D-EPR mapping measurements.

The developed software solution is a working prototype, and it is expected that it will be improved by further development. So far it complies with the main tasks: to control the instrumentation of the FRaScan HFEPR spectrometer and to perform automated measurement routines. During the development, several requirements changed or were added. A few unexpected inconveniences made it difficult to implement for example a carousel holder and the frequency rapid-scan in a current solution. However, potential ways for their implementation have already been explored. In the case of the carousel holder, the control of the piezo motor will require finishing work on its LabVIEW driver. The incompatibility issue of digitizer's ADQAPI with LabVIEW can be workaround via a wrapper library written in C, or by using the *LabVIEW memory manager* functions that can perform low-level operations such as dynamically allocating, manipulating, and releasing memory. The *power monitor* can be implemented by reading status signals on a serial line (RS-232) adapter. According to *the Riello Sentinel Pro* manual, pins 9 and 8 indicate *operation on battery* and *low battery* respectively. Some UPS equipped with a USB port behave as a plug-and-play device that is recognized by the operating system as a battery. Then reading of *system power status* bits through a kernel of an operating system provides sufficient information about the status of UPS for evaluation of next operations. The architecture of the software may be also reformed. In the ideal case, the commanding module shall be divided into several modules: a Top GUI, a Measurement executor, an Instrument server, an Event logger, and a Data logger. The Top GUI should only present data to the user and handle user actions. The Measurement executor should only manage measurement procedures. The Instrument server would receive commands from the Top GUI or Measurement executor and interpret them to the submodules responsible for the operation of individual instruments or subsystems. Also, it should process data from submodules and interpret them to the Top GUI or Measurement

executioner. The submodules that control the actual instruments can be implemented with multiple abstraction layers to decrease the coupling between the Instrument server and particular instrument.

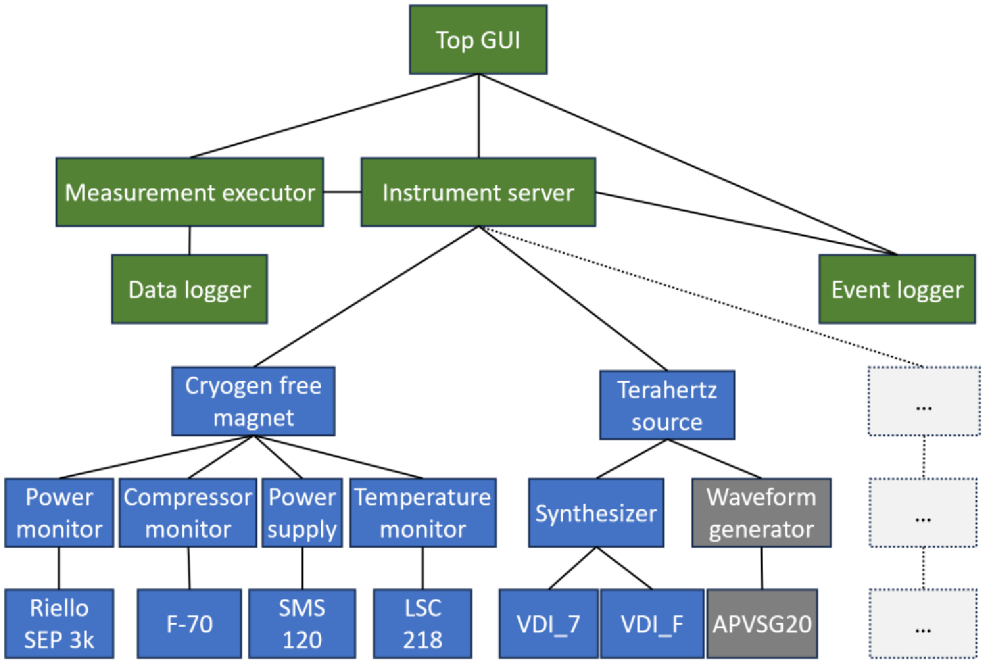

Figure 21: Suggested architecture of improved software solution.

3.5 Implementation of frequency rapid scan

While the quasi-optical system and the terahertz system allow the spectrometer to operate in a broad frequency range and obtain EPR spectra by frequency sweeping, to enable the frequency rapid scan operation, only a few modifications were done.

To be able to perform frequency rapid scan (FRaScan) measurements on various samples, a vector signal generator APVSG20 from AnaPico AG (Switzerland, Glattbrugg) was added. It can generate a signal of arbitrary profile in the frequency range 0.01 – 20 GHz. The generator is controlled via an application provided by AnaPico, but waveform data are generated by a MATLAB script.

To upgrade a signal acquisition in the built HFEPR spectrometer by needs of a frequency rapid scan operation, an ADQ7 digitizer from Teledyne SP devices, with an optional advanced time-domain firmware (FWATD) and PXIe form factor, was used. It has input bandwidth DC - 3 GHz with a sampling rate of 10 GS/s in single-channel mode, or 5 GS/s in dual-channel mode. The ADQ7 was supplied with a software development kit (SDK). Unfortunately, a LabVIEW driver is not part of the SDK and provided ADQAPI.dll, is not completely compatible with the LabVEIW. Moreover, the FWATD was never meant to be used with a LabVIEW. Due to this obstacle, the Digitizer module was not fully implemented in the main software solution and the rapid scan experiments were done using a MATLAB script written by Oleksii Laguta.

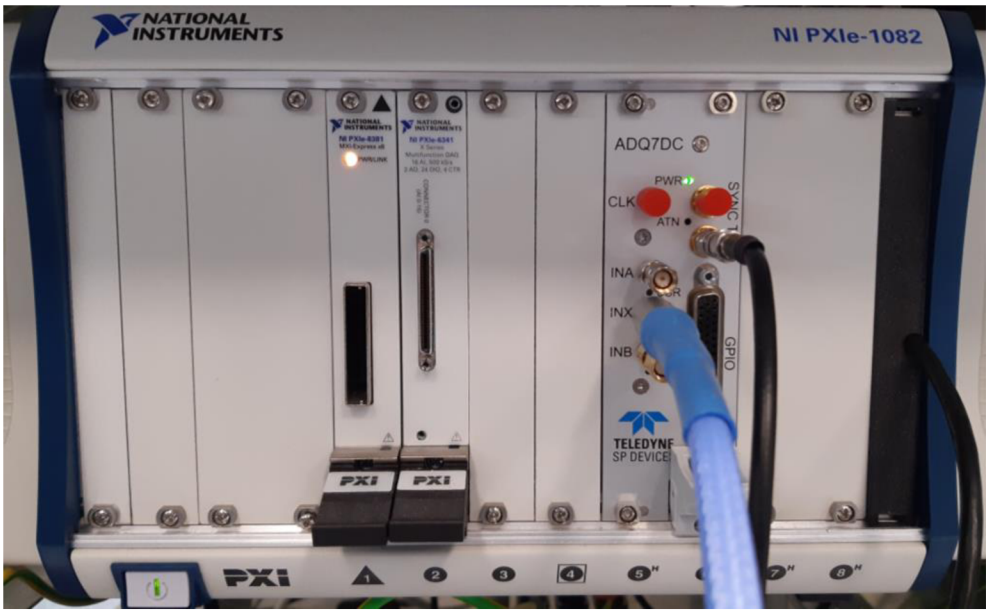

Figure 22: PXIe chassis with ADQ7DC in a single channel mode. The digitizer is connected to PC via USB3.0 on the right side of the chassis. (MXI and GPIO cards are currently not used.)

The modulation coil of the SSH was used to add an offset to the external magnetic field around a sample. This is done to acquire rapid scan EPR spectra when the field is set in the resonance, and background signal when it is out of the resonance conditions. The background signal is caused by the frequency-dependent behavior of all components in the path of the microwave signal. To get the doble offset of magnetic field, polarity of the direct electric current is simply change. In our case, the source meter unit Keithley 2450 was used for this purpose. The source meter has triaxial output connectors at its rear panel. A pair of adapters and standard 50Ω coaxial cables were used for the connection of leads between the source meter and the probe head, which minimized external interference.

4 Solid state materials studied by HF-EPR

The solid-state paramagnetic species provides information about site symmetry, electronic configuration, and neighboring atoms. The complexity arises from anisotropies that needs to be included to the spin Hamiltonian to describe the spin system.

Among many applications of EPR is research of defects in solid state materials that has potential for improvement of quality assessment in semiconductor industry, progress in development of spintronic devices and quantum computing [5]. In further subsections of this chapter will be shown measured spectra of selected paramagnetic species in semiconductors obtained by the developed HFEPR FRaScan spectrometer. Other published results which includes data from the spectrometer are: EDMR spectra of nitrogen-doped 15R SiC, [62, 72], HFEPR spectra of SIMs based on Co(II) complexes [73, 74], EPR maps of copper acetate hydrate [75], FS-EPR spectra of ^{14}N-TEMPOL and CW-EPR spectra of iron(II) phthalocyanine (FePc) [61], rapid scan spectra of LiPc [33] and EPR maps of $Mn_{12}Ac$ [76], all of which were performed using the software developed in this thesis.

4.1 HF-EPR study of SiC doped by Vanadium

In this chapter, HFEPR measurements and analysis of chosen crystal materials will be described. The first chosen sample is a 4H-SiC doped by Vanadium (SiC:V). The vanadium substitutes Si atoms in the SiC lattice in one of three charge states and behaves as an amphoteric impurity. In the charge state V^{4+} the vanadium acts neutral, while in V^{3+} and V^{5+} it acts as an acceptor or donor respectively [77]. Therefore, it compensates for residual impurities that are commonly present in grown SiC crystals, and its amphoteric behavior is used for the fabrication of semi-insulating substrates in high-power microwave electronics [78].

With the assumption that the residual impurity is for example a nitrogen (donor), the oxidation state of the vanadium dopant regardless of the site is V^{3+} with a spin $S = 1$ [78]. The vanadium then creates two inequivalent paramagnetic centers with different properties, one in the quasicubic site and the second in the hexagonal site of the SiC crystal. Spectra of the both paramagnetic centers will be split due to the zero-field interaction since S=1. Furthermore, the naturally predominant isotope 51V with a natural abundance of 99.75 % has nuclear spin $I = 7/2$, and therefore each EPR absorption peak displays $2I+1 = 8$ lines arising from the hyperfine splitting. This means that the four mentioned absorption peaks further split into 8 hyperfine lines. The EPR spectra of 4H-SiC:V then shall contain four groups of 8 lines, while the four groups originate from a zero-field splitting (D) and two possible lattice sites (hexagonal and quasicubic) [79].

Two samples of SiC:V (photo on Figure 23) were obtained from Jan Kunc from Charles University in Prague. Both samples were cut off from the same 4H-SiC wafer,

with the concentration of V dopants estimated by secondary ion mass spectroscopy to $3 \cdot 10^{17}$ cm^{-3} [77]..

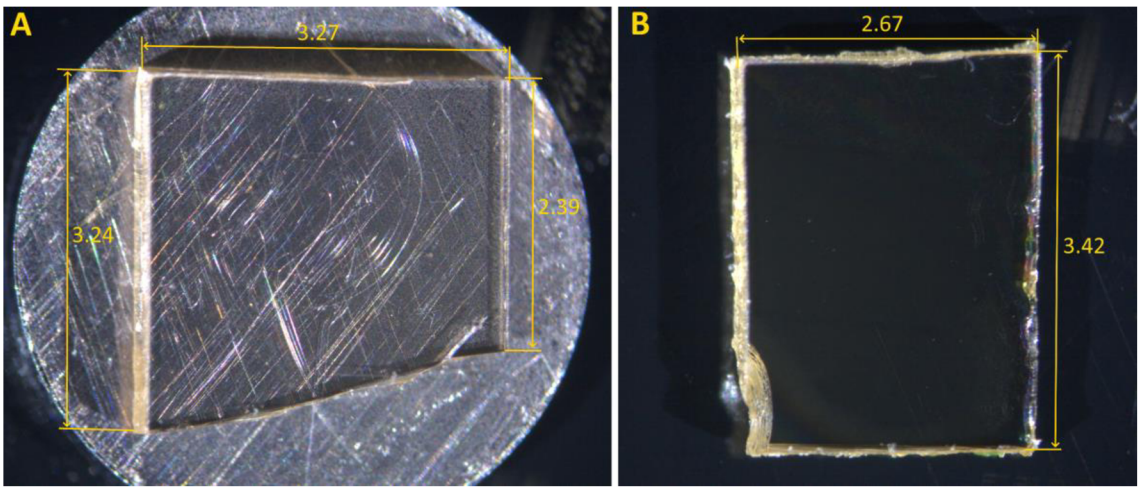

Figure 23: Two samples of 4H-SiC:V cut from a wafer. The sample A with area ~9.2 mm^2 is placed on a mirror, sample B with area ~9.1 mm^2 is in a sample box with black background.

First, a series of CW-EPR measurements were performed on sample A, placed the SSH. Starting from the temperature of sample 16 K, the CW-EPR spectra were obtained at 283.07, 316.5, and 349.9 GHz. Then measurements were repeated at increasing temperature, up to 140 K to check the behavior of the paramagnetic centers. From these measurements, three representative spectra measured with microwave excitation at a frequency of 349.9 GHz are plotted in Figure 24.

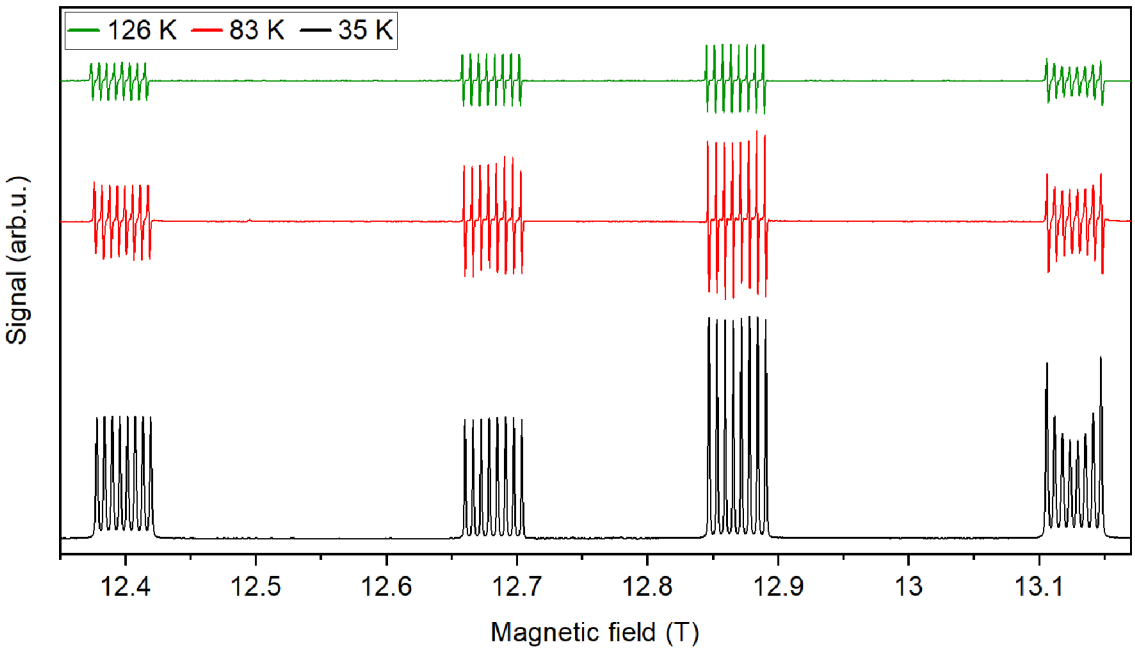

Figure 24: Temperature dependency of 4H-SiC:V CW-EPR spectra at 349.9 GHz. (ramp rate: 1 mT/s,modulation: 3 G at 10 kHz, low pass filter time constant: 150 ms, intensity was corrected based on noise level sampled at 12.5-12.6 T)

Further, frequency-dependent spectra at 65 K are shown in Figure 25. An apparent increase in the signal intensity at higher resonance frequencies is caused by a bigger

difference in energy levels resulting in a larger difference in the population of states (equation 12 on page 8).

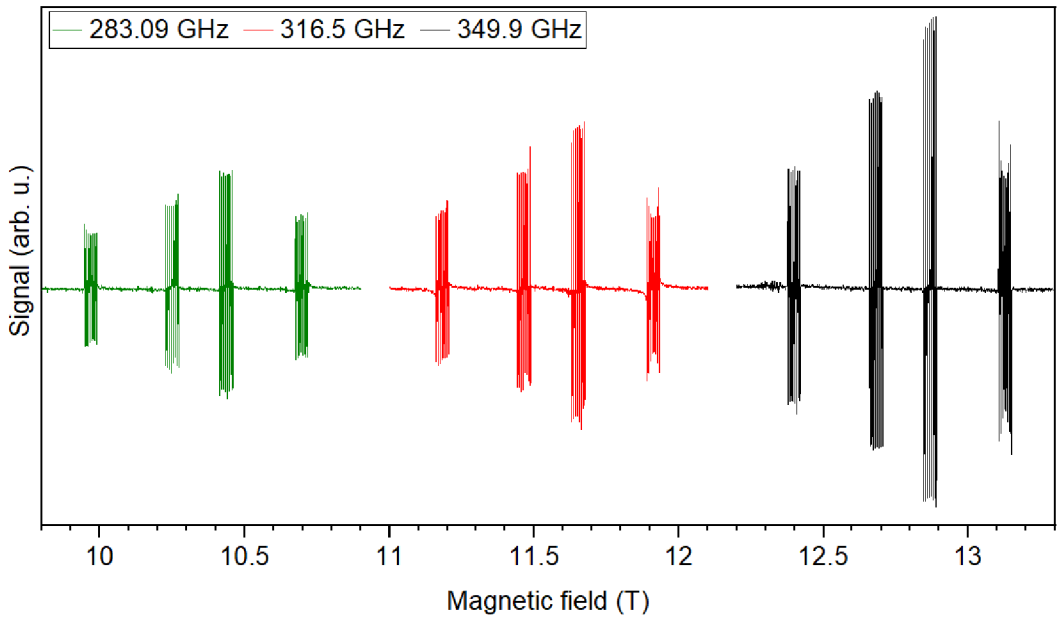

Figure 25: Frequency dependence of 4H-SiC: V cw-EPR spectra at 65 K. (Parameters are same as for temperature dependency on Figure 22. Intensity correction: 0.778: 1: 0.186)

4.2 FS-EPR measurements and EPR maps

Two examples of 2D-EPR maps are in Figure 26 and Figure 27. Both were obtained by stacking non-averaged FS-EPR spectra during a continuous field sweep. The field range was set to start and end the magnetic sweep out of resonance. FS-EPR spectra that are out of resonance were used to subtract the background from the whole dataset of a 2D-EPR map by applying equation:

$$s_c(i) = s_o(i) - b_s + \left(\frac{i}{n}\right) \cdot (b_s - b_e) \tag{26}$$

Where b_s and b_e are background pattern at the start and the end border of the magnetic field sweep, s_c is the corrected signal, s_o is the original signal, b_s and b_e are the backgrounds at the start and end respectively in the dataset, i is the iterator through field domain, n is the total number of FS-EPR scans. Despite the fact that the magnetic field ramp rate was set to the lowest possible by the current hardware, 0.1789 mT/s, the resulting number of scans was too low and CW-EPR spectra could not be recovered in sufficient quality. There were also regions in which was not possible to distinguish all peaks from the FS-EPR spectra and faster frequency sweeps would lead to limiting parameters which would result in poor SNR. Anyway, it was possible to extract partial FS-EPR spectra (marked by colored dot lines in Figure 26-A) for each set of lines with were centered around 288 GHz (Figure 26-C) and 307.5 GHz (Figure 26-B).

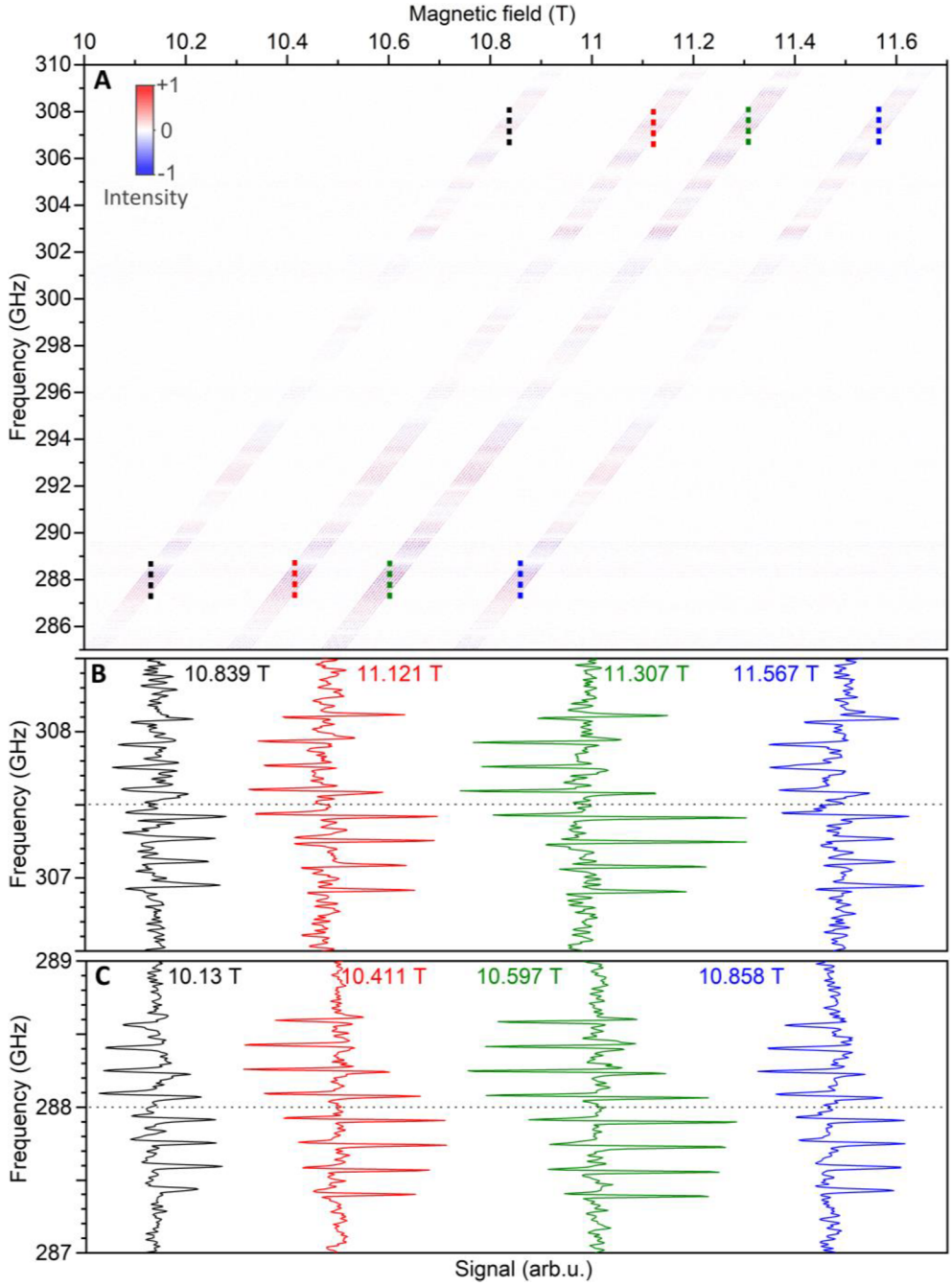

Figure 26: A) Broad 2D-EPR map of 4H-SiC:V. Doted colored lines denotes position of extracted particular FS-EPR spectra. B) Particular FS-EPR spectra for each set of lines that were centred at 307.5 GHz. C) Particular FS-EPR spectra for each set of lines that were centred at 288 GHz.

Table 1:Parameters for acquisition of 2D-EPR map in relatively broad range.

Frequency range	282 – 312 GHz	Field range	9.5 – 12 T
Sweep rate	7.3242 GHz/s	Ramp rate	0.17893 mT/s
Modulation frequency	6 kHz	Modulation amplitude	~ 3 G
Low-pass filter constant	~ 0.25 ms	Sample temperature	~ 80 K
FS-EPR record length	60 000 points	Number of scans	3048

A similar procedure was followed to make a map in Figure 27-A but in this case, the map has a much higher resolution in the magnetic field domain (4779 points). It was achieved by a shorter frequency sweep in a narrower range, while the magnetic field ramp rate was set as low as the power supply for the magnet allowed (0.1789 mT/s). There were enough data points to recover CW-EPR spectra of sufficient quality for further analysis. Two spectra were recovered from the frequencies 292.14 and 294.26 GHz, and plotted in Figure 27-B.

Table 2: Parameters for acquisition of 2D-EPR map in relatively narrow range.

Frequency range	292 – 294.5 GHz	Field range	10 – 11.3 T
Sweep rate	2.4414 GHz/s	Ramp rate	0.17893 mT/s
Modulation frequency	6 kHz	Modulation amplitude	~ 2.5 G
Low-pass filter constant	~ 4.1 ms	Sample temperature	~ 81 K
FS-EPR record length	15 000 points	Number of scans	4779

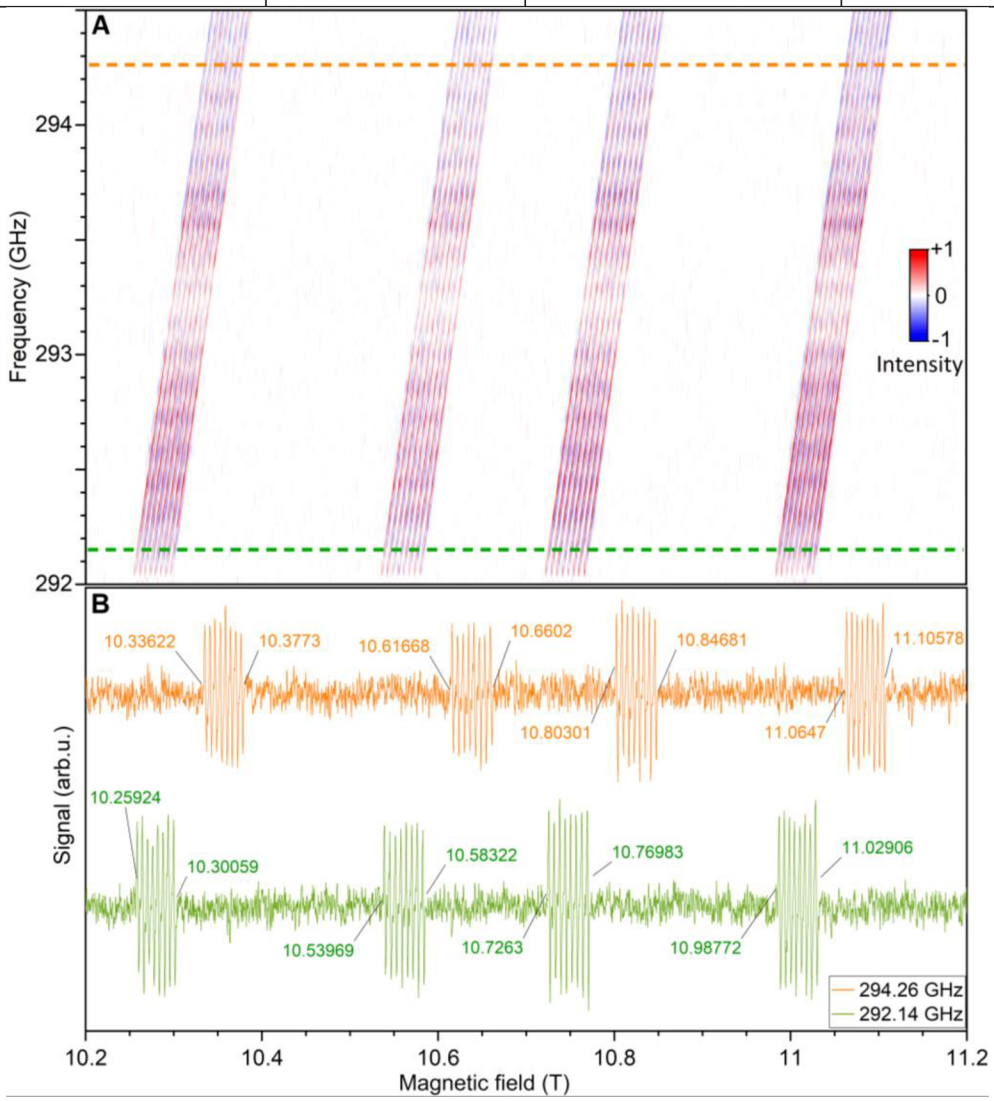

Figure 27: A) 2D-EPR made of 4779 FS-EPR scans at rate 2.44 GHz/s during continuous field sweep at rate 0.179 mT/s. Filter constant 4ms, modulation frequency 6 kHz, modulation amplitude 2.5 G, datapoints in frequency domain - 15 000, 81 K. B) Extracted CW spectra from the map.

4.3 Rotation measurements

By rotating crystals in the magnetic field, the anisotropic behavior of the EPR spectra of paramagnetic species can be studied. Attempt to do this with 4H-SiC: V unfortunately did not bring satisfying results. The EPR signals were too low in intensity to resolve and distinguish from a background. Moreover, at such low temperatures (~65 K), other signals appeared either from contamination, trapped air bubbles, or defects in the sapphire rod of the rotator. For this reason, it was decided to provide an example of the sample of lithium phthalocyanine (LiPc) at room temperature. The sample is a needle-shaped crystal, and the axis of symmetry is the long axis of needles. The LiPc is a molecule that possesses one unpaired electron, resulting in a radical with a spin of S = 1/2 and displays weak anisotropy [80–82]. By rotation of LiPc crystal in the magnetic field and measuring the EPR spectra, the g tensor parallel and perpendicular to the long axes of the crystal was determined. The sample was placed in the rotator equipped with the Teflon rod, perpendicular to the axis of rotation. Doing this in CW mode would be time-consuming. Instead, we used the FS-EPR to obtain 321 spectra with a step of 1° rotation.

Table 3: Parameters for FS-EPR rotational map measuremnts of LiPc crystal.

Frequency sweep range	216.05 – 216.15 [GHz]	Static magnetic field	7.7 T
Sweep time	1.024 s	VTI temperature	280 K
Modulation frequency	10 kHz	Modulation amplitude	~ 0.1 G
Low-pass filter constant	~ 0.1 ms	Record length	15 000 points
Averaging	4 scans	Rotator range	2 – 322 °
Rotator step	1°	Delay between step	3 s

All obtained spectra were processed in OriginPro software [83] and assembled into an FS-EPR rotational map plotted in Figure 28. The data were fit with parameters $g_{\perp}$= 2.00529 and $g_{\parallel}$= 2.00533 via angular-dependent simulation in EasySpin [43]. However, this result may vary from values in the literature [80, 84], because of the relatively large instrumental uncertainty of the used superconducting magnet (~15 mT).

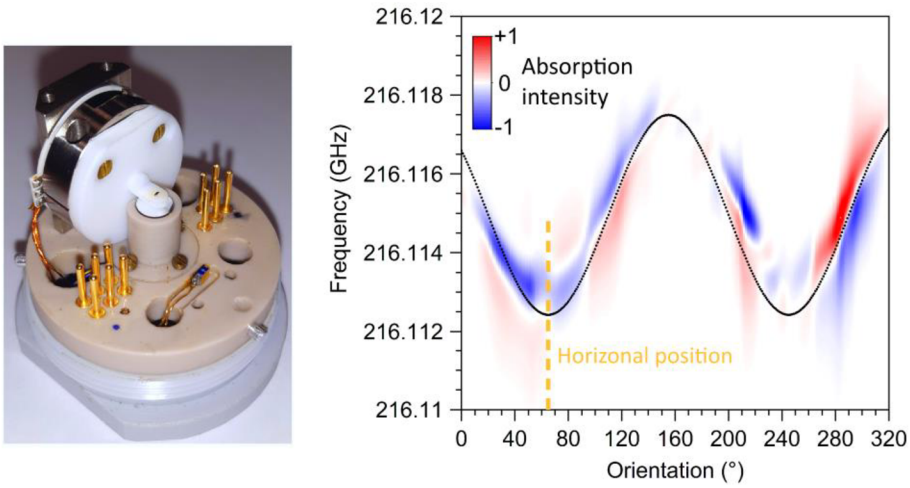

Figure 28: Left - Rotator sample holder with LiPc crystal placed on PTFE rod. Right - Rotational map made of 321 FS-EPR spectra, by 1° step. Measured at room temperature and magnetic field of 7.7 T. Orange dashed line denotes a position in which crystal axis is parallel to XY-plane and perpendicular to magnetic field (~65 °). Published in [85].

4.4 FRaScan measurements

To test the FRaScan capabilities of the spectrometer a trial measurement on a crystal sample of 1,3-bisdiphenylene-2-phenylallyl (BDPA) was performed. The BDPA is commonly used in EPR spectroscopy as a molecular standard, and its g-factor is ~2.003 [86].

To generate frequency scans, we used APVSG20 and the AMCs with the multiplication factor 9. The scan range was 100.5 – 101.3 GHz, and the rate was 0.4 MHz/ns (400 THz/s ≈ 14.27 MT/s). The period of the scans was 2 µs. The magnetic field was set to ~3.6 T, and the temperature of the sample to 70 K. The digitizer was set to acquire 40 000 samples at a rate of 10 GS/s (two sweep periods) and perform 250 000 averages (accumulations). The data acquisition took about 1 second. On the left side of Figure 29 is plotted a portion of data that contains the rapid scan signal along with the background signal that was recorded when the magnetic field was shifted out of the resonance. On the right side is just the rapid scan signal cleared of the background by subtraction. The maxima of each oscillation in the rapid scan spectrum were fitted by an exponential function and from the signal decay a relaxation time of T_2^*≈27.6 ns was estimated. From the intensity of the first peak and standard deviation of the signal in the 600–700 ns region was estimated the SNR of ~1096.

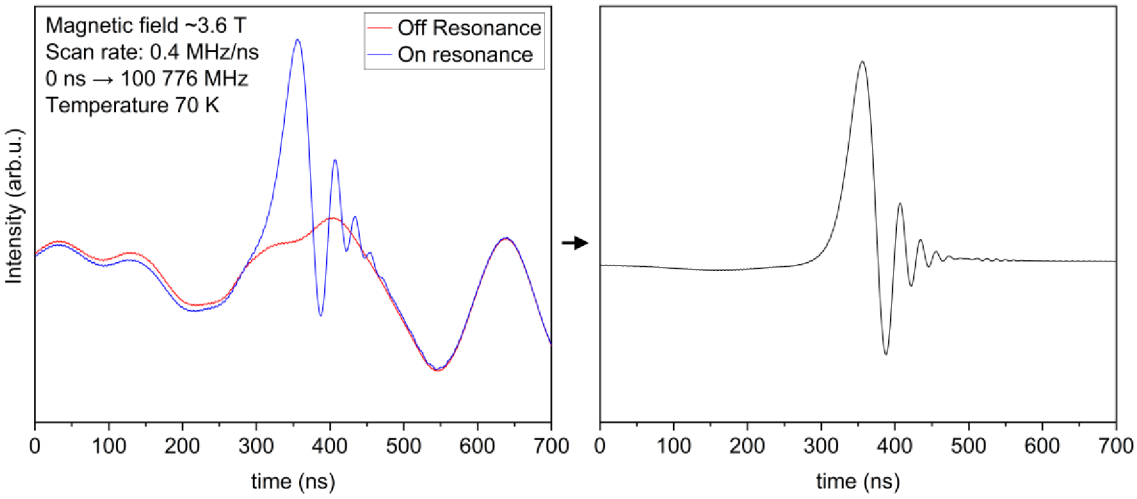

Figure 29: FRaScan performed on crystal of BDPA at temperature of 70 K. On the left side is raw acquiered spectra (on resonance) and its bacground (off resonace. On the right side is the FRaScan spectra clean of the bacground.

Conclusion

The outcomes demonstrate the successful implementation of the FRaScan HFEPR spectrometer. It allows to study of a broad variety of samples, via the conventional CW-EPR method at multiple frequencies at hundreds of gigahertz, and under controlled conditions. It also implements the FS-EPR and a novel frequency rapid scan method. The data produced by the spectrometer has already influenced multiple publications [33, 61, 62, 72–76, 87], with more about to come. The developed software was reported in the Journal of Magnetic Resonance [85]. Automation of measurements significantly decreases the amount of time that would be otherwise spent by the operator performing experiments. The source code of the software is publicly available via the GitHub repository at https://github.com/MatSevy/CEITEC-HFEPR-spectrometer-LV under a GNU GPL v3 license. Other researchers (not only from the EPR community) can download it, modify its source code for their needs, or just take inspiration from it. However, there are still many possibilities to improve the spectrometer in terms of hardware and software.

On the hardware side, there is still some room to improve the sample holders. For example, the simple sample holder currently cannot use a local heater and magnetic field sensor at the same time. A simple solution for this is to extend its connector by one pair of contacts. The use of different materials could help distribute heat from the heater to the sample while keeping the sample holder thermally isolated from the probe. The rotator sample holder suffers from a significant drop in the signal which could be improved by redesigning its waveguide. Also, different materials for the shaft should be tried. In the carousel sample holder, the encoded needs to be debugged. Improved airflow around the digitizer in the PXIe chassis can reduce its temperature and extend its life.

On the software side, the architecture of the software can be further improved by the insertion of an intermediate abstraction layer to submodules, and the division of the supervising module into multiple entities. To simplify the implementation of new features and extensions, the application of object-oriented programming should be considered. Submodules for lock-in amplifiers, and magnetic field sensors can be further improved. Also, a submodule for carousel sample holder control needs to be implemented into the main software. Also monitoring the compressor's operation and UPS state should be added. The software for the FRaScan HFEPR spectrometer could be extended to support also the FTIR spectrometer. The submodule for the digitizer will first require a proper driver that shall be done as a collection of wrapper VIs above ADQAPI.dll, while some VIs will need to be modified by a low-level LabVIEW Manager function. Also, a new module for the signal generator needs to be implemented, to be able to generate faster frequency sweeps with a custom sweep profile.

Literature references

[1] RANGUELOVA, Kalina. *EPR-The „workhorse technique" that is still enabling scientists to break new ground after 70+ years* [online]. 2017 [vid. 2022-12-27]. Dostupné z: https://www.europeanpharmaceuticalreview.com/wp-content/uploads/BBS.R.098-EPR-Whitepaper_LayoutFULL-1.pdf

[2] RALPH T. WEBER. *Modern EPR Applications From Beer to DEER* [online]. Rheinstetten (Germany): Bruker BioSpin Corp. EPR Division. 2011 [vid. 2022-12-27]. Dostupné z: https://www.cif.iastate.edu/sites/default/files/uploads/EPR/ModernEPRapps.pdf

[3] EPEL, Boris, Gage REDLER a Howard J. HALPERN. How in vivo epr measures and images oxygen. *Advances in Experimental Medicine and Biology* [online]. 2014, **812**, 113–119 [vid. 2022-12-27]. ISSN 22148019. Dostupné z: doi:10.1007/978-1-4939-0620-8_15/COVER

[4] SATHIYA, M., J. B. LERICHE, E. SALAGER, D. GOURIER, J. M. TARASCON a H. VEZIN. Electron paramagnetic resonance imaging for real-time monitoring of Li-ion batteries. *Nature Communications 2015 6:1* [online]. 2015, **6**(1), 1–7 [vid. 2022-12-27]. ISSN 2041-1723. Dostupné z: doi:10.1038/ncomms7276

[5] LIU, Junjie, Valentin LAGUTA, Katherine INZANI, Weichuan HUANG, Sujit DAS, Ruchira CHATTERJEE, Evan SHERIDAN, Sinéad M. GRIFFIN, Arzhang ARDAVAN a Ramamoorthy RAMESH. Coherent electric field manipulation of Fe3+ spins in PbTiO3. *Science Advances* [online]. 2021, **7**(10), 1–8. ISSN 23752548. Dostupné z: doi:10.1126/sciadv.abf8103

[6] PRIVITERA, Alberto, Ross WARREN, Giacomo LONDI, Pascal KAIENBURG, Junjie LIU, Andreas SPERLICH, Andreas E. LAURITZEN, Oliver THIMM, Arzhang ARDAVAN, David BELJONNE a Moritz RIEDE. Electron spin as fingerprint for charge generation and transport in doped organic semiconductors. *Journal of Materials Chemistry C* [online]. 2021, **9**(8), 2944–2954. ISSN 20507526. Dostupné z: doi:10.1039/d0tc06097f

[7] ASTAKHOV, Oleksandr, Lihong XIAO, Friedhelm FINGER, Tao CHEN, Matthias FEHR, Benjamin GEORGE, Alexander SCHNEGG, Klaus LIPS a Christian TEUTLOFF. Multifrequency EPR study of HWCVD μc-SiC:H for photovoltaic applications. *physica status solidi (a)* [online]. 2016, **213**(7), 1747–1750 [vid. 2022-12-27]. ISSN 1862-6319. Dostupné z: doi:10.1002/PSSA.201533027

[8] CICCULLO, Francesca, Mathias GLASER, Marie S. SÄTTELE, Samuel LENZ, Petr NEUGEBAUER, Yvonne RECHKEMMER, Joris VAN SLAGEREN a M. Benedetta CASU. Thin film properties and stability of a potential molecular

quantum bit based on copper(II). *Journal of Materials Chemistry C* [online]. 2018, **6**(30), 8028–8034 [vid. 2022-12-27]. ISSN 2050-7534. Dostupné z: doi:10.1039/C8TC02610F

[9] GOPHANE, Dnyaneshwar B., Burkhard ENDEWARD, Thomas F. PRISNER a Snorri Th SIGURDSSON. A semi-rigid isoindoline-derived nitroxide spin label for RNA. *Organic & Biomolecular Chemistry* [online]. 2018, **16**(5), 816–824 [vid. 2022-12-27]. ISSN 1477-0539. Dostupné z: doi:10.1039/C7OB02870A

[10] ZHANG, Peng, Mauro PERFETTI, Michal KERN, Philipp P. HALLMEN, Liviu UNGUR, Samuel LENZ, Mark R. RINGENBERG, Wolfgang FREY, Hermann STOLL, Guntram RAUHUT a Joris VAN SLAGEREN. Exchange coupling and single molecule magnetism in redox-active tetraoxolene-bridged dilanthanide complexes. *Chemical Science* [online]. 2018, **9**(5), 1221–1230 [vid. 2022-12-27]. ISSN 2041-6539. Dostupné z: doi:10.1039/C7SC04873D

[11] SALIKHOV, K. M. a N. E. ZAVOISKAYA. Zavoisky and the discovery of EPR. *Resonance* [online]. 2015, **20**(11), 963–968 [vid. 2022-12-27]. ISSN 0973712X. Dostupné z: doi:10.1007/S12045-015-0264-6/METRICS

[12] BAKER, Michael. Brebis Bleaney. *Physics Today* [online]. 2007, **60**(3), 80 [vid. 2022-12-27]. ISSN 0031-9228. Dostupné z: doi:10.1063/1.2718768

[13] PRISNER, T. F., S. UN a R. G. GRIFFIN. Pulsed ESR at 140 GHz. *Israel Journal of Chemistry* [online]. 1992, **32**(2–3), 357–363 [vid. 2023-11-27]. ISSN 1869-5868. Dostupné z: doi:10.1002/IJCH.199200042

[14] GHIM, Barnard T., Jing Long DU, Susanne PFENNINGER, George A. RINARD, Richard W. QUINE, Sandra S. EATON a Gareth R. EATON. Multifrequency electron paramagnetic resonance of irradiated l-alanine. *Applied Radiation and Isotopes* [online]. 1996, **47**(11–12), 1235–1239 [vid. 2023-11-27]. ISSN 0969-8043. Dostupné z: doi:10.1016/S0969-8043(96)00037-1

[15] SCHLECKER, Benedikt, Alexander HOFFMANN, Anh CHU, Maurits ORTMANNS, Klaus LIPS a Jens ANDERS. Towards Low-Cost, High-Sensitivity Point-of-Care Diagnostics Using VCO-Based ESR-on-a-Chip Detectors. *IEEE Sensors Journal* [online]. 2019, **19**(20), 8995–9003 [vid. 2023-11-23]. ISSN 15581748. Dostupné z: doi:10.1109/JSEN.2018.2875767

[16] JOSHI, Janhavi P., John R. BALLARD, George A. RINARD, Richard W. QUINE, Sandra S. EATON a Gareth R. EATON. Rapid-scan EPR with triangular scans and fourier deconvolution to recover the slow-scan spectrum. *Journal of Magnetic Resonance* [online]. 2005, **175**(1), 44–51 [vid. 2022-10-20]. ISSN 1090-7807. Dostupné z: doi:10.1016/J.JMR.2005.03.013

[17] WEIL, John A. a James R. BOLTON. *Electron Paramagnetic Resonance: Elementary Theory and Practical Applications, Second Edition* [online]. B.m.: Wiley-Interscience, 2006. ISBN 9780471754961. Dostupné z: doi:10.1002/9780470084984

[18] WEBER, Y. Ralph. An EPR Primer. In: *Xenon User's Guide* [online]. Billerica (MA): Bruker BioSpin Corporation, 2011 [vid. 2022-12-27]. Dostupné z: https://www.cif.iastate.edu/sites/default/files/uploads/EPR/CW%20EPR%20Primer(XenonSoftware).pdf

[19] EATON, Gareth R., Sandra S. EATON, David P. BARR a Ralph T. WEBER. *Quantitative EPR* [online]. 1. vyd. Viena: Springer, 2010 [vid. 2022-12-27]. ISBN 9783211929476. Dostupné z: doi:10.1007/978-3-211-92948-3/COVER

[20] DUIN, Evert. Basic EPR Theory. In: *Electron Paramagnetic Resonance Theory (course manual)* [online]. nedatováno [vid. 2022-12-27], s. 1–42. Dostupné z: https://webhome.auburn.edu/~duinedu/epr/1_theory.pdf

[21] MISRA, Sushil K. *Multifrequency Electron Paramagnetic Resonance: Theory and Applications* [online]. B.m.: Wiley-VCH, 2011 [vid. 2022-12-27]. ISBN 9783527407798. Dostupné z: doi:10.1002/9783527633531

[22] SCHWEIGER, Arthur a Gunnar JESCHKE. *Principles of pulse electron paramagnetic resonance*. Oxford: Oxford University Press, 2001. ISBN 9780198506348.

[23] DUIN, Evert. Practical Aspects . In: *lectron Paramagnetic Resonance Theory* [online]. Auburn (AL): Auburn University, nedatováno [vid. 2022-12-28]. Dostupné z: https://webhome.auburn.edu/~duinedu/epr/2_pracaspects.pdf

[24] HRUSZOWIEC, Mariusz, Kacper NOWAK, Bogusław SZLACHETKO, Michał GRZELCZAK, Wojciech CZARCZYŃSKI, Edward F PLIŃSKI a Tadeusz WIĘCKOWSKI. The Microwave Sources for EPR Spectroscopy. *Journal of Telecommunications and Information Technology* [online]. 2017, **2**, 18–25 [vid. 2022-12-28]. Dostupné z: https://www.itl.waw.pl/czasopisma/JTIT/2017/2/18.pdf

[25] CHARLES P. POOLE. *Electron spin resonance: a comprehensive treatise on experimental techniques* [online]. 2nd vyd. Mineola, N.Y.: Dover Publications, 1996 [vid. 2022-10-20]. ISBN 0486694445. Dostupné z: https://books.google.com/books/about/Electron_Spin_Resonance.html?hl=cs&id=P-4PIoi7Z7IC

[26] NASH, Eamon. *UNDERSTANDING, OPERATING, AND INTERFACING TO INTEGRATED DIODE-BASED RF DETECTORS* [online]. 2015 [vid. 2022-12-28]. Dostupné z: https://www.analog.com/en/technical-articles/integrated-diode-based-rf-detectors.html

[27] TSEITLIN, M. P., V. S. IYUDIN a O. A. TSEITLIN. Advantages of digital phase-sensitive detection for upgrading an obsolete CW EPR spectrometer. *Applied Magnetic Resonance* [online]. 2009, **35**(4), 569–580 [vid. 2022-12-28]. ISSN 09379347. Dostupné z: doi:10.1007/S00723-009-0186-0/METRICS

[28] R. CAMMACK AND J.K. SHERGILL. EPR SPECTROSCOPY OF PROTEINS. In: *Proteins labfax* [online]. San Diego (CA): BIOS Scientific Publishers, 1996 [vid. 2023-12-18], s. 217–231. ISBN 9780125647106. Dostupné z: https://search.worldcat.org/title/301231066

[29] KRSTIĆ, Ivan, Burkhard ENDEWARD, Dominik MARGRAF, Andriy MARKO a Thomas F. PRISNER. Structure and dynamics of nucleic acids. In: *EPR spectroscopy - Applications in Chemistry and Biology* [online]. B.m.: Springer, Berlin, Heidelberg, 2011 [vid. 2023-12-12], s. 159–198. ISBN 9783642283468. Dostupné z: doi:10.1007/128_2011_300/COVER

[30] WEBER, Ralph T. *Pulsed EPR Primer* [online]. Billerica (MA): Bruker Instruments, 2000 [vid. 2022-12-28]. Dostupné z: http://www.sb.fsu.edu/~fajer/Fajerlab/LinkedDocuments/Primer.pdf

[31] DELIGIANNAKIS, Yiannis, Maria LOULOUDI a Nick HADJILIADIS. Electron spin echo envelope modulation (ESEEM) spectroscopy as a tool to investigate the coordination environment of metal centers. *Coordination Chemistry Reviews* [online]. 2000, **204**(1), 1–112 [vid. 2023-12-20]. ISSN 0010-8545. Dostupné z: doi:10.1016/S0010-8545(99)00218-0

[32] A. SCHWEIGER AND G. JESCHKE. *Principles of Pulse Electron Paramagnetic Resonance. Oxford University Press* [online]. Oxford: Oxford University Press, 2001 [vid. 2024-01-08]. ISBN 0198506341. Dostupné z: https://books.google.com/books/about/Principles_of_Pulse_Electron_Paramagneti.html?hl=cs&id=tkvQQElkW1wC

[33] LAGUTA, O., A. SOJKA, A. MARKO a P. NEUGEBAUER. Rapid scan ESR: A versatile tool for the spin relaxation studies at (sub)THz frequencies. *Applied Physics Letters* [online]. 2022, **120**(12), 120502 [vid. 2022-12-08]. ISSN 0003-6951. Dostupné z: doi:10.1063/5.0083010

[34] TSEYTLIN, Mark. General solution for rapid scan EPR deconvolution problem. *Journal of Magnetic Resonance* [online]. 2020, **318**, 106801 [vid. 2024-01-10]. ISSN 1090-7807. Dostupné z: doi:10.1016/J.JMR.2020.106801

[35] TSEITLIN, Mark, George A. RINARD, Richard W. QUINE, Sandra S. EATON a Gareth R. EATON. Deconvolution of sinusoidal rapid EPR scans. *Journal of Magnetic Resonance* [online]. 2011, **208**(2), 279–283 [vid. 2023-05-11]. ISSN 1090-7807. Dostupné z: doi:10.1016/J.JMR.2010.11.015

[36] HYDE, James S., Robert A. STRANGEWAY, Theodore G. CAMENISCH, Joseph J. RATKE a Wojciech FRONCISZ. W-band frequency-swept EPR. *Journal of Magnetic Resonance* [online]. 2010, **205**(1), 93–101 [vid. 2024-01-09]. ISSN 1090-7807. Dostupné z: doi:10.1016/J.JMR.2010.04.005

[37] NGUYEN, Doan N., James MICHEL a Chuck H. MIELKE. Status and Development of Pulsed Magnets at the NHMFL Pulsed Field Facility. *IEEE*

Transactions on Applied Superconductivity [online]. 2016, **26**(4) [vid. 2023-05-11]. ISSN 10518223. Dostupné z: doi:10.1109/TASC.2016.2515982

[38] ZHERLITSYN, S., B. WUSTMANN, T. HERRMANNSDÖRFER a J. WOSNITZA. Magnet-technology development at the dresden high magnetic field laboratory. *Journal of Low Temperature Physics* [online]. 2013, **170**(5–6), 447–451 [vid. 2023-05-11]. ISSN 00222291. Dostupné z: doi:10.1007/S10909-012-0764-7/FIGURES/2

[39] *EPR Software Suites: From Acquisition through Processing and Simulation* [online]. Billerica (MA): Bruker BioSpin. 2019 [vid. 2022-12-28]. Dostupné z: https://www.bruker.com/en/products-and-solutions/mr/epr-instruments/epr-software.html

[40] WEBER, Ralph. *Xenon Data Processing Reference* [online]. Billerica (MA USA): Bruker BioSpin, 2012. Dostupné z: http://www.nmrcenter.buffalo.edu/EPR_Processing.pdf

[41] BORIS EPEL. *SpecMan4EPR* [online]. Chicago (IL): FeMi Instruments. 2017 [vid. 2022-12-28]. Dostupné z: www.specman4epr.com

[42] EPEL, Boris, Igor GROMOV, Stefan STOLL, Arthur SCHWEIGER a Daniella GOLDFARB. Spectrometer manager: A versatile control software for pulse EPR spectrometers. *Concepts in Magnetic Resonance Part B: Magnetic Resonance Engineering* [online]. 2005, **26B**(1), 36–45 [vid. 2023-01-12]. ISSN 1552-504X. Dostupné z: doi:10.1002/CMR.B.20037

[43] STOLL, Stefan a Arthur SCHWEIGER. EasySpin, a comprehensive software package for spectral simulation and analysis in EPR. *Journal of Magnetic Resonance* [online]. 2006, **178**(1), 42–55. ISSN 10907807. Dostupné z: doi:10.1016/j.jmr.2005.08.013

[44] TAIT, Claudia E., Matthew D. KRZYANIAK a Stefan STOLL. Computational tools for the simulation and analysis of spin-polarized EPR spectra. *Journal of Magnetic Resonance* [online]. 2023, **349**, 107410 [vid. 2024-01-11]. ISSN 1090-7807. Dostupné z: doi:10.1016/J.JMR.2023.107410

[45] WANG, Qiuliang, Zhipeng NI, Chunyan CUI, Qiuliang WANG, Zhipeng NI a Chunyan CUI. Superconducting Magnet Technology and Applications. In: *Superconductors - Materials, Properties and Applications* [online]. B.m.: IntechOpen, 2012 [vid. 2023-01-02]. ISBN 978-953-51-0794-1. Dostupné z: doi:10.5772/48465

[46] KRAMER DAVID. Helium shortage has ended, at least for now. *Physics Today* [online]. 2020, **2020**(2) [vid. 2023-01-02]. ISSN 0031-9228. Dostupné z: doi:10.1063/PT.6.2.20200605A

[47] SMIRNOV, Alex I., Tatyana I. SMIRNOVA, Ryan L. MACARTHUR, Jeremy A. GOOD a Renny HALL. Cryogen-free superconducting magnet system for

multifrequency electron paramagnetic resonance up to 12.1 T. *Review of Scientific Instruments* [online]. 2006, **77**(3). ISSN 00346748. Dostupné z: doi:10.1063/1.2182571

[48] REIJERSE, E., P. P. SCHMIDT, G. KLIHM a W. LUBITZ. A CW and pulse EPR spectrometer operating at 122 and 244 GHz using a quasi-optical bridge and a cryogen-free 12 T superconducting magnet. *Applied Magnetic Resonance 2007 31:3* [online]. 2007, **31**(3), 611–626 [vid. 2022-12-12]. ISSN 1613-7507. Dostupné z: doi:10.1007/BF03166606

[49] UDAL, Andres, Martin JAANUS, Gintaras VALUŠIS, Irmantas KAŠALYNAS, Zoran IKONIC a Dragan INDJIN. Progress in development of the resonant tunneling diodes as promising compact sources at the THz gap bottom. *NATO Science for Peace and Security Series B: Physics and Biophysics* [online]. 2017, **PartF1**, 169–178 [vid. 2023-01-02]. ISSN 18746500. Dostupné z: doi:10.1007/978-94-024-1093-8_20

[50] HORNSTEIN, M. K., R. G. GRIFFIN, J. MACHUZAK, M. A. SHAPIRO, R. J. TEMKIN a K. E. KREISCHER. A 460 GHz gyrotron oscillator for use in DNP / NMR spectroscopy. *IEEE International Conference on Plasma Science* [online]. 2001 [vid. 2023-01-02]. ISSN 07309244. Dostupné z: doi:10.1109/PPPS.2001.961319

[51] MEHDI, I., G. CHATTOPADHYAY, E. SCHLECHT, J. WARD, J. GILL, F. MAIWALD a A. MAESTRINI. Terahertz multiplier circuits. *IEEE MTT-S International Microwave Symposium Digest* [online]. 2006, 341–344 [vid. 2023-01-02]. ISSN 0149645X. Dostupné z: doi:10.1109/MWSYM.2006.249521

[52] PRAJAPATI, Dhruvi D a Neelkanthan USHA. Review Paper on Frequency Multiplier at Terahertz Range. *International Journal on Recent and Innovation Trends in Computing and Communication* [online]. 2017, **5**(2), 228–232 [vid. 2023-01-02]. ISSN 2321-8169. Dostupné z: doi:10.17762/IJRITCC.V5I2.204

[53] LIU, Xiao-Yu, 刘晓宇, Yong ZHANG, 张勇, De-Jiao XIA, 夏德娇, Tian-Hao REN, 任田昊, Jing-Tao ZHOU, 周静涛, Dong GUO, 郭栋, Zhi JIN a 金智. A High-Sensitivity Terahertz Detector Based on a Low-Barrier Schottky Diode*. *Chinese Physics Letters* [online]. 2017, **34**(7), 070701 [vid. 2023-01-02]. ISSN 0256-307X. Dostupné z: doi:10.1088/0256-307X/34/7/070701

[54] REIJERSE, Edward J. High-frequency EPR instrumentation. *Applied Magnetic Resonance* [online]. 2010, **37**(1), 795–818 [vid. 2022-10-20]. ISSN 09379347. Dostupné z: doi:10.1007/S00723-009-0070-Y

[55] *Bolometers and IR Detectors - IRLabs* [online]. [vid. 2024-01-12]. Dostupné z: https://www.irlabs.com/products/bolometers/

[56] EFETOV, Dmitri K., Ren Jye SHIUE, Yuanda GAO, Brian SKINNER, Evan D. WALSH, Hyeongrak CHOI, Jiabao ZHENG, Cheng TAN, Gabriele GROSSO, Cheng PENG, James HONE, Kin Chung FONG a Dirk ENGLUND. Fast thermal relaxation in cavity-coupled graphene bolometers with a Johnson noise read-out. *Nature Nanotechnology 2018 13:9* [online]. 2018, **13**(9), 797–801 [vid. 2023-01-02]. ISSN 1748-3395. Dostupné z: doi:10.1038/s41565-018-0169-0

[57] GOLDSMITH, Paul F. Quasi-Optical Techniques. *Proceedings of the IEEE* [online]. 1992, **80**(11), 1729–1747 [vid. 2023-01-02]. ISSN 15582256. Dostupné z: doi:10.1109/5.175252

[58] SMITH, G. M., J. C.G. LESURF, R. H. MITCHELL a P. C. RIEDI. Quasi-optical cw mm-wave electron spin resonance spectrometer. *Review of Scientific Instruments* [online]. 1998, **69**(11), 3924 [vid. 2022-11-10]. ISSN 0034-6748. Dostupné z: doi:10.1063/1.1149200

[59] NEUGEBAUER, Petr a Anne Laure BARRA. New cavity design for broad-band quasi-optical hf-epr spectroscopy. *Applied Magnetic Resonance* [online]. 2010, **37**(1), 833–843 [vid. 2021-03-22]. ISSN 09379347. Dostupné z: doi:10.1007/s00723-009-0092-5

[60] NAFTALY, M., R.E. MILES a P.J. GREENSLADE. THz transmission in polymer materials — a data library. *2007 Joint 32nd International Conference on Infrared and Millimeter Waves and the 15th International Conference on Terahertz Electronics* [online]. 2007, 819–820 [vid. 2024-01-18]. Dostupné z: doi:10.1109/ICIMW.2007.4516747

[61] SOJKA, Antonín, Matúš ŠEDIVÝ, Adam LAGIN, Andrej GABRIS, Tomáš LÁZNIČKA, Vinicius Tadeu SANTANA, Oleksii LAGUTA a Petr NEUGEBAUER. Sample Holders for Sub-THz Electron Spin Resonance Spectroscopy. *IEEE Transactions on Instrumentation and Measurement* [online]. 2022, **71** [vid. 2022-10-13]. ISSN 15579662. Dostupné z: doi:10.1109/TIM.2022.3164135

[62] SOLODOVNYK, Artur, Dariya SAVCHENKO, Oleksii LAGUTA a Petr NEUGEBAUER. Implementation of Broadband Electrically Detected Magnetic Resonance in a sub-THz FraScan Spectrometer. *IEEE Transactions on Instrumentation and Measurement* [online]. 2023 [vid. 2023-08-02]. ISSN 15579662. Dostupné z: doi:10.1109/TIM.2023.3284951

[63] KALKMAN, Cor J. LabVIEW: A software system for data acquisition, data analysis, and instrument control. *Journal of Clinical Monitoring* [online]. 1995, **11**(1), 51–58 [vid. 2021-05-17]. ISSN 07481977. Dostupné z: doi:10.1007/BF01627421

[64] ELLIOTT, Chance, Vipin VIJAYAKUMAR, Wesley ZINK a Richard HANSEN. National Instruments LabVIEW: A Programming Environment for Laboratory Automation and Measurement. *Journal of Laboratory Automation*

[online]. 2007, **12**(1), 17–24 [vid. 2021-05-17]. ISSN 15402452. Dostupné z: doi:10.1016/j.jala.2006.07.012

[65] SOJKA, Antonín. *Development of a Novel Terahertz Magnetic Resonance Spectrometer for Spin Dynamics Investigations* [online]. B.m., 2022. Brno University of Technology. Dostupné z: https://dspace.vutbr.cz/handle/11012/204114

[66] ST MARIE, Luke, Abdel EL FATIMY, Jakub HRUBÝ, Ivan NEMEC, James HUNT, Rachael MYERS-WARD, D. KURT GASKILL, Mattias KRUSKOPF, Yanfei YANG, Randolph ELMQUIST, Raphael MARX, Joris VAN SLAGEREN, Petr NEUGEBAUER a Paola BARBARA. Nanostructured graphene for nanoscale electron paramagnetic resonance spectroscopy. *Journal of Physics: Materials* [online]. 2020, **3**(1), 014013 [vid. 2023-11-09]. ISSN 2515-7639. Dostupné z: doi:10.1088/2515-7639/AB6AF8

[67] MARTYNIUK, Oleh, Vivek CHAUDHARY, M. BARTOŠ, O. LAGUTA, Rachael MYERS-WARD, D Kurt GASKILL, P. BARBARA, A. EL FATIMY a Petr NEUGEBAUER. Graphene Quantum Dot Bolometer Camera: Practical Approaches and Preliminary Results. *2023 48th International Conference on Infrared, Millimeter, and Terahertz Waves (IRMMW-THz)* [online]. 2023, 1–2 [vid. 2023-11-09]. Dostupné z: doi:10.1109/IRMMW-THZ57677.2023.10298959

[68] COLLE, Jean Yves, Jouni RAUTIO a Daniel FREIS. A modular LabVIEW application frame for Knudsen Effusion Mass Spectrometry instrument control. *SoftwareX* [online]. 2021, **16**, 100875 [vid. 2022-02-24]. ISSN 23527110. Dostupné z: doi:10.1016/j.softx.2021.100875

[69] TITOV, Igor. Using LabVIEW for building laboratory server: Pros and cons, design patterns, software architecturing and common pitfalls. *IEEE Global Engineering Education Conference, EDUCON* [online]. 2014, (April), 1101–1107. ISSN 21659567. Dostupné z: doi:10.1109/EDUCON.2014.6826247

[70] FABIOLA DE LA CUEVA. *Delacor Queued Message Handler* [online]. 2022 [vid. 2023-08-31]. Dostupné z: https://dqmh.org/

[71] CZERWINSKI, Fabian a Lene B. ODDERSHEDE. TimeSeriesStreaming.vi: LabVIEW program for reliable data streaming of large analog time series. *Computer Physics Communications* [online]. 2011, **182**(2), 485–489 [vid. 2022-10-18]. ISSN 0010-4655. Dostupné z: doi:10.1016/J.CPC.2010.10.019

[72] SOLODOVNYK, Artur, Oleksii LAGUTA, Andrey PROKHOROV, Michele SEGANTINI, Boris NAYDENOV, Petr NEUGEBAUER, Siegmund GREULICH-WEBER, Ekaterina KALABUKHOVA a Dariia SAVCHENKO. Spin dynamics of exchange-coupled nitrogen donors in heavily doped n -type 15R SiC monocrystals: Multifrequency EPR and EDMR study. *Physical Review B* [online]. 2023, **107**(15), 155202 [vid. 2023-08-02]. ISSN 24699969. Dostupné z: doi:10.1103/PHYSREVB.107.155202

[73] GIRALDO, Jorge Navarro, Jakub HRUBÝ, Šárka VAVREČKOVÁ, Ondřej F. FELLNER, Lubomír HAVLÍČEK, Da Vonne HENRY, Shehan DE SILVA, Radovan HERCHEL, Miroslav BARTOŠ, Ivan ŠALITROŠ, Vinicius T. SANTANA, Paola BARBARA, Ivan NEMEC a Petr NEUGEBAUER. Tetracoordinate Co(II) complexes with semi-coordination as stable single-ion magnets for deposition on graphene. *Physical Chemistry Chemical Physics* [online]. 2023, **25**(43), 29516–29530 [vid. 2024-01-15]. ISSN 1463-9084. Dostupné z: doi:10.1039/D3CP01426F

[74] JURÁKOVÁ, Jana, Ondřej F. FELLNER, Sören SCHLITTENHARDT, Šárka VAVREČKOVÁ, Ivan NEMEC, Radovan HERCHEL, Erik ČIŽMÁR, Vinicius Tadeu SANTANA, Milan ORLITA, Denis GENTILI, Giampiero RUANI, Massimiliano CAVALLINI, Petr NEUGEBAUER, Mario RUBEN a Ivan ŠALITROŠ. Neutral cobalt(II)-bis(benzimidazole)pyridine field-induced single-ion magnets for surface deposition. *Inorganic Chemistry Frontiers* [online]. 2023, **10**(18), 5406–5419 [vid. 2024-01-15]. ISSN 2052-1553. Dostupné z: doi:10.1039/D3QI00931A

[75] CALVO, Rafael, Rosana P. SARTORIS, Otaciro R. NASCIMENTO, Matúš ŠEDIVÝ, Antonin SOJKA, Petr NEUGEBAUER a Vinicius T. SANTANA. Quantum phase transitions probed by EPR spectra in dimeric spin arrays with supramolecular couplings. *Coordination Chemistry Reviews* [online]. 2023, **480**, 215007 [vid. 2023-02-14]. ISSN 0010-8545. Dostupné z: doi:10.1016/J.CCR.2022.215007

[76] SOJKA, Antonín, Matúš ŠEDIVÝ, Oleksii LAGUTA, Andriy MARKO, Vinicius T. SANTANA a Petr NEUGEBAUER. High-frequency EPR: Current state and perspectives. *Electron Paramagnetic Resonance* [online]. 2021, **27**, 214–252 [vid. 2022-10-12]. ISSN 14651955. Dostupné z: doi:10.1039/9781839162534-00214

[77] REJHON, Martin, Mykola BRYNZA, Roman GRILL, Eduard BELAS a Jan KUNC. Investigation of deep levels in semi-insulating vanadium-doped 4H-SiC by photocurrent spectroscopy. *Physics Letters, Section A: General, Atomic and Solid State Physics* [online]. 2021, **405**, 127433 [vid. 2022-05-26]. ISSN 03759601. Dostupné z: doi:10.1016/j.physleta.2021.127433

[78] MITCHEL, W. C., W. D. MITCHELL, G. LANDIS, H. E. SMITH, Wonwoo LEE a M. E. ZVANUT. Vanadium donor and acceptor levels in semi-insulating 4H - And 6H-SiC. *Journal of Applied Physics* [online]. 2007, **101**(1). ISSN 00218979. Dostupné z: doi:10.1063/1.2407263

[79] VON BARDELEBEN, Hans Jürgen, S. A. ZARGALEH, J. L. CANTIN, Weibo. B. GAO, Timur BIKTAGIROV a Uwe GERSTMANN. Transition metal qubits in 4H -silicon carbide: A correlated EPR and DFT study of the spin S=1 vanadium V3+ center. *Physical Review Materials* [online]. 2019, **3**(12), 124605

[vid. 2022-10-20]. ISSN 24759953. Dostupné z: doi:10.1103/PHYSREVMATERIALS.3.124605/

[80] SATO, Hideo, Lauraine A. DALTON, Duc HA, Richard W. QUINE, Sandra S. EATON a Gareth R. EATON. Electron Spin Relaxation in x-Lithium Phthalocyanine. *Journal of Physical Chemistry B* [online]. 2007, **111**(28), 7972–7977 [vid. 2022-12-21]. ISSN 15206106. Dostupné z: doi:10.1021/JP070810Y

[81] WACHTEL, H., J. C. WITTMANN, B. LOTZ, M. A. PETIT a J. J. ANDRÉ. Anisotropic spin transport in oriented lithium phthalocyanine thin films. *Thin Solid Films* [online]. 1994, **250**(1–2), 219–231 [vid. 2022-12-20]. ISSN 0040-6090. Dostupné z: doi:10.1016/0040-6090(94)90189-9

[82] AFEWORKI, Mobae, Nathan R. MILLER, Nallathamby DEVASAHAYAM, John COOK, James B. MITCHELL, S. SUBRAMANIAN a Murali C. KRISHNA. Preparation and EPR Studies of Lithium Phthalocyanine Radical as an Oxymetric Probe. *Free Radical Biology and Medicine* [online]. 1998, **25**(1), 72–78 [vid. 2022-12-20]. ISSN 0891-5849. Dostupné z: doi:10.1016/S0891-5849(98)00039-2

[83] *OriginPro*. Northampton, MA, USA: OriginLab Corp. 2022

[84] BRINKMANN, M. a J. J. ANDRÉ. Electrodeposited lithium phthalocyanine thin films. Part II:† magnetic properties and mesoscopic effects. *Journal of Materials Chemistry* [online]. 1999, **9**(7), 1511–1520 [vid. 2022-12-21]. ISSN 1364-5501. Dostupné z: doi:10.1039/A809778J

[85] ŠEDIVÝ, Matúš, Vinicius SANTANA, Antonín SOJKA, Oleksii LAGUTA a Petr NEUGEBAUER. MEPROS – Modular electron paramagnetic resonance operating software for multifunctional high-frequency EPR spectrometer. *Journal of Magnetic Resonance* [online]. 2023, **355**, 107556 [vid. 2024-01-16]. ISSN 1090-7807. Dostupné z: doi:10.1016/J.JMR.2023.107556

[86] KÜNSTNER, Silvio, Anh CHU, Klaus Peter DINSE, Alexander SCHNEGG, Joseph E. MCPEAK, Boris NAYDENOV, Jens ANDERS a Klaus LIPS. Rapid-scan electron paramagnetic resonance using an EPR-on-a-Chip sensor. *Magnetic Resonance* [online]. 2021, **2**(2), 673–687 [vid. 2024-01-17]. ISSN 26990016. Dostupné z: doi:10.5194/MR-2-673-2021

[87] MIDLÍKOVÁ, Jana Dubnická, Matúš ŠEDIVÝ, Antonín SOJKA, Vinicius Tadeu SANTANA, Adam DUBROKA a Petr NEUGEBAUER. A Versatile Setup for Fourier-Transform Infrared Magneto-Spectroscopy. *IEEE Transactions on Instrumentation and Measurement* [online]. 2023, **72**, 1–11 [vid. 2023-07-26]. ISSN 0018-9456. Dostupné z: doi:10.1109/TIM.2023.3284943